Turkish Journal of Earth Sciences

http://journals.tubitak.gov.tr/earth/

Research Article

Turkish J Earth Sci
(2020) 29: 257-279

doi:10.3906/yer-1904-25

Geochemistry and mineralogy of the shallow subsurface Red Sea coastal sediments, Rabigh, Saudi Arabia: provenance and paleoenvironmental implications

Rabea HAREDY[1], **Ibrahim GHANDOUR**[1,2,*]

[1]Department of Marine Geology, Faculty of Marine Science, King Abdulaziz University, Jeddah, Saudi Arabia
[2]Department of Geology, Faculty of Science, Tanta University, Tanta, Egypt

Received: 30.04.2019 • **Accepted/Published Online:** 30.10.2019 • **Final Version:** 15.01.2020

Abstract: Mineralogical and geochemical characteristics of the shallow subsurface sediments retrieved from a short sediment core (2.05 m long) collected from the tidal flat south of Al-Kharrar Lagoon, Rabigh area, Saudi Arabia, are presented to determine the impact of temporal change of depositional environment and distinguish the principal control(s) on their chemical composition. The sediments are dominantly siliciclastic, consisting of two vertically stacked sedimentary facies: lagoonal (LG) gray silt-rich mud to argillaceous very fine sand at the base and intertidal flat (TF) brown mud and argillaceous very fine-grained sands at the top. The sediments of the two facies are similar in their mineralogical and chemical composition except for slight vertical variations in the relative abundance of minerals and concentrations of major oxides and trace elements. The mineralogical composition is dominated by quartz, feldspars, and plagioclase with less abundant clay minerals and hornblende, all of detrital origin. In addition, traces of high and low Mg-calcite, dolomite, and gypsum were recognized. Geochemically, the sediments are first-cycle and compositionally immature. The Al_2O_3/TiO_2 ratios range from 9.4 to 17 and from 13 to 15.4 for the sediments of the LG and TF facies, respectively. These values suggest an intermediate igneous source rock of the Birak group that belongs to the oceanic island arc of the Hijaz Terrane, western Arabian Shield. The average values of paleoweathering indices CIA, CIW, and PIA are <50, suggesting unweathered to poorly weathered source rock that is consistent with the late Holocene arid climate. Although the redox-sensitive V and Cr in the sediments of LG facies are slightly enriched relative to the average shale, the values of the V/Cr ratio are generally <2, suggesting deposition under oxic conditions. The chemical characteristics of the sediments are primarily controlled by the composition of source rock and to a lesser extent by hydraulic sorting during transportation and deposition.

Key words: Sediment geochemistry, paleoweathering, hydraulic sorting, Hijaz Terrane, Red Sea coastal plain

1. Introduction

Source-rock composition and interrelated processes, including the climate-induced weathering, hydraulic sorting, postdepositional alterations, and environmental conditions, are the fundamental factors that work individually or mutually to determine the mineralogical and chemical composition of sediments (Ohta and Arai, 2007; Yan et al., 2012; Reotita et al., 2014; Guo et al., 2018; Ghandour and Haredy, 2019; Ghandour et al., 2019; Tribovillard et al., 2019). Multiple geochemical proxies have been utilized to decipher the dominant control(s) on sediment geochemistry (e.g., Cruces et al., 2006; Sawant et al., 2017). Temporal variations in depositional environments may be accompanied by variations in the chemical composition of the ambient sediments because each environment has its own physical and chemical processes. The change of these processes may leave an imprint on the sediment mineralogical and chemical composition. However, environmental interpretations relying on geochemical proxies should be treated carefully because of the complex interplay with other parameters, particularly provenance variations.

The Red Sea coastal lagoons that were formed by Holocene transgression (Rasul, 2015) have experienced environmental perturbations and readjustments attributed to sea level and climatic changes (Abu-Zied and Bantan, 2015; Bantan et al., 2019; Ghandour and Haredy, 2019). These lagoons provide an undisturbed and continuous sedimentary record that can be used to reconstruct the Holocene environmental and climatic fluctuations and events. The late Holocene paleoenvironmental changes have been interpreted using vertical variations in sedimentary facies and micropaleontological and geoarchaeological analysis (Bailey et al., 2007; Hein et al., 2011; Abu-Zied and Bantan, 2015; Ghandour et al., 2016; Bantan et al., 2019; Ghandour and Haredy,

* Correspondence: ighandour@kau.edu.sa

2019). Notably, the use of sediment mineralogy and geochemistry to pinpoint the impact of such perturbations and environmental changes has not been explored yet. The depositional evolution of the shallow subsurface sediments of the tidal flat south of Al-Kharrar Lagoon, Rabigh area, Saudi Arabia, is well constrained based on sedimentary facies analysis (Ghandour and Haredy, 2019). Two vertically sedimentary facies were recognized: a lagoonal facies at the base sharply overlain by a tidal flat facies at the top. The objectives of the present study are to determine the mineralogical and chemical composition of the sediments previously interpreted by Ghandour and Haredy (2019) in order to determine their potential for provenance and paleoenvironment interpretations and to distinguish the dominant factor(s) on geochemical characteristics. This approach has been successfully applied for the Holocene sediments in the Nile Delta (Siegel et al., 1995), Mediterranean (Martin-Puertas et al., 2010; Marco-Barba et al., 2013), south Yellow Sea (Lü et al., 2016), South China Sea (Cui et al., 2016; Ge et al., 2019), and Tanzanian shelf (Liu et al., 2017). The findings of this work will help to understand the geochemical evolution of Al-Kharrar Lagoon in relation to the late Holocene sea level and climate.

2. Study area

The area of study covers the southern tidal flat of the Al-Kharrar Lagoon, North Rabigh city (Figure 1). The area was tectonically stable and undisturbed during the Quaternary. The Al-Kharrar Lagoon is a coastal water body connected to the Red Sea through a narrow inlet. It is 18 km long, 4.86 km at maximum width, and 14 m in maximum depth and it covers an area of 71.44 km^2 (Rasul, 2015). The western and southern coasts contain mangroves (*Avicennia marina*) (Rasul, 2015). The bottom sediments of the lagoon consist of a mixture of land-derived siliciclastic detritus and calcareous skeletal remains displaying heterogeneous distribution, where the southern and eastern shallow nearshore areas contain abundant siliciclastic sand and mud grains (Basaham, 2008; Rasul, 2015; Hariri and Abu-Zied, 2018). The bottom sediments of the internal part of the lagoon comprise calcareous skeletal remains (Rasul, 2015).

The southern tidal flat of the Al-Kharrar Lagoon receives sediments from the rocks of the Arabian Shield and the Cenozoic sedimentary and volcanic rocks exposed to the east of the Rabigh area (Figure 2) through the temporarily active Wadi Rabigh (Zaigham et al., 2015). The western part of the Arabian Shield is composed primarily of four Neoproterozoic tectonostratigraphic terranes representing the earliest formed rocks in the shield, mostly of oceanic crust affinity (intraoceanic island arc). These terranes from north to south are the Midyan, Hijaz, Jiddah, and Asir (Johnson et al., 2003; Hargrove et al., 2006; Bamousa, 2013). The Hijaz terranes along with other terranes in the western part of the Arabian Shield are the earliest formed rocks in the shield and mostly originated in the juvenile Neoproterozoic oceanic environment.

The Neoproterozoic Hijaz and Jeddah arc terranes that flank the Bi'r Umq Suture Zone (BUSZ) in western Saudi Arabia record some of the earliest magmatic and deformational events in the juvenile part of the Arabian Nubian Shield (ANS). The Arabian Shield consists of assemblages of calc-alkaline volcanic and intrusive igneous rocks developed as magmatic arcs at convergent boundaries. These rocks include basalt, andesite, rhyolite, diorite, tonalite, and granodiorite. The Hijaz Terrane includes three amalgamated stratotectonic units: the Farri marginal basin, the Birak volcanic complex, and the Al Ays volcanic complex (Johnson, 2006). The Birak group represents oceanic-floor to continental-slope deposits. It consists of low K-tholeiitic volcanic and volcaniclastic sedimentary rocks (Ramsay, 1986; Johnson et al., 2003). Wadi Rabigh originates from the Hijaz Terrane and flows westward and northwestward, discharging directly into the Red Sea or indirectly through Al-Kharrar Lagoon.

The Al-Kharrar Lagoon is strongly influenced by northerly wind-generated waves, currents, aeolian action, and limited tidal currents, with negligible wadi (alluvial) flow. The wind-generated currents and waves control the movement of both water and sediments to the adjacent tidal flat, particularly during winter and high tides. A relatively wide and low-gradient tidal flat bordering the southern shoreline of the lagoon is cut by shallow channels that are flooded for several hundreds of meters during spring tides augmented by the active wind. The tidal flat is covered locally by algal (cyanobacterial) mats with a tufted and honeycomb morphology. The lower tidal flat is disturbed by active crab burrowing (Ghandour and Haredy, 2019). Most of the previous studies carried out in the study area focused on the foraminiferal distribution and the textural, mineralogical, and geochemical characteristics of the Al-Kharrar Lagoon bottom sediments (e.g., Abou-Ouf, 1996; Al-Washmi, 1999; Basaham, 2008; Basaham et al., 2015; Al-Dubai et al., 2017; Hariri and Abu-Zied, 2018). The subsurface stratigraphy of the eastern and southern coastal plain of the Al-Kharrar Lagoon was briefly described (Behairy et al., 1991; El Abd and Awad, 1991). Behairy et al. (1991) recognized four siliciclastic-dominated strata arranged from top to bottom as 1) relatively thin mud and sand layers containing evaporite minerals, 2) yellowish-brown sand and mud, 3) gray sand and mud, and 4) gravel-rich deposits. The lithology of the shallow subsurface sediments beneath the tidal flat surrounding the Al-Kharrar Lagoon differs spatially; it is calcareous to the north and siliciclastic to the south. Relying on

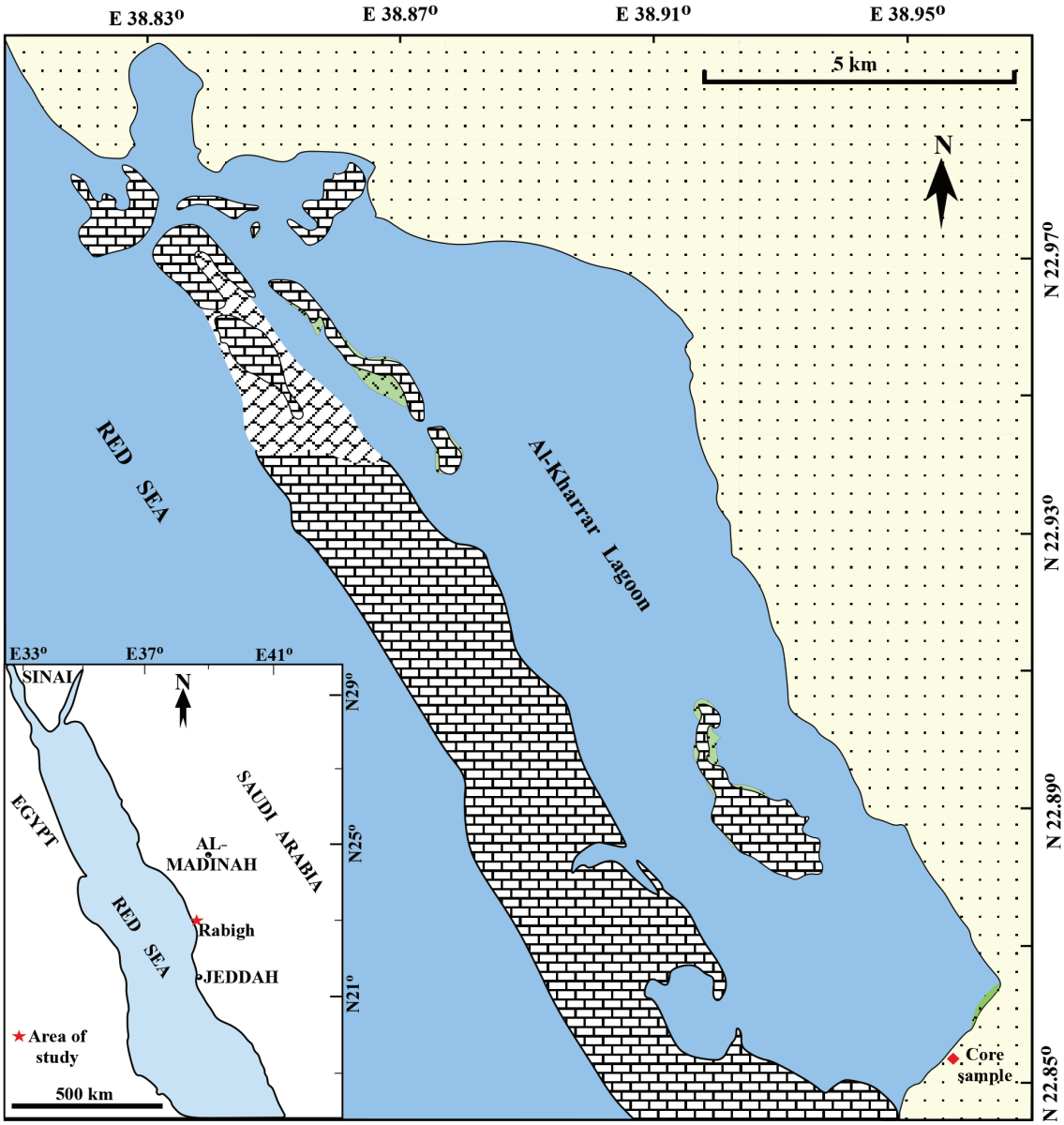

Figure 1. Location map of the study area showing the location of the core.

the downcore variations in sediment composition, the paleotidal elevation curve, and the benthic foraminifera record from a short sediment core (2.25 m long) collected from the intertidal area of NE Al-Kharrar Lagoon, Bantan et al. (2019) recently reconstructed paleoenvironmental conditions and sea-level changes over the last 5500 years. They recorded fluctuations in the depositional environment from inter- to subtidal and the vertical variation of the benthic foraminiferal record distinguishes two warming events (AD 750–1500 and 1750–present) enclosing a cooling event during AD 1500–1750. Ghandour and Haredy (2019) subdivided the shallow subsurface siliciclastic-dominated sediments of the tidal flat south of Al-Kharrar Lagoon (Figure 3) into the gray mud and argillaceous fine sands of lagoonal origin (LG) in the lower flat (depth 54 to 205 cm) and the upper brown mud and argillaceous fine-grained sands (0–54 cm from the top) interpreted as an intertidal flat (TF). The mean grain size of the sediments of the LG facies varied from 13 to 83 μm (silt to very fine sands) with an average of 45 μm. The sand content varies from 2% to 67% with an average of 31%, whereas the silt content varies between 32% and 87% with an average of 63%. The clay content is generally less than 11%. The mean grain size varies in the sediments of TF facies between 34 and 80 μm (silt and very fine sands) with an average of 42 μm. The sand content varies

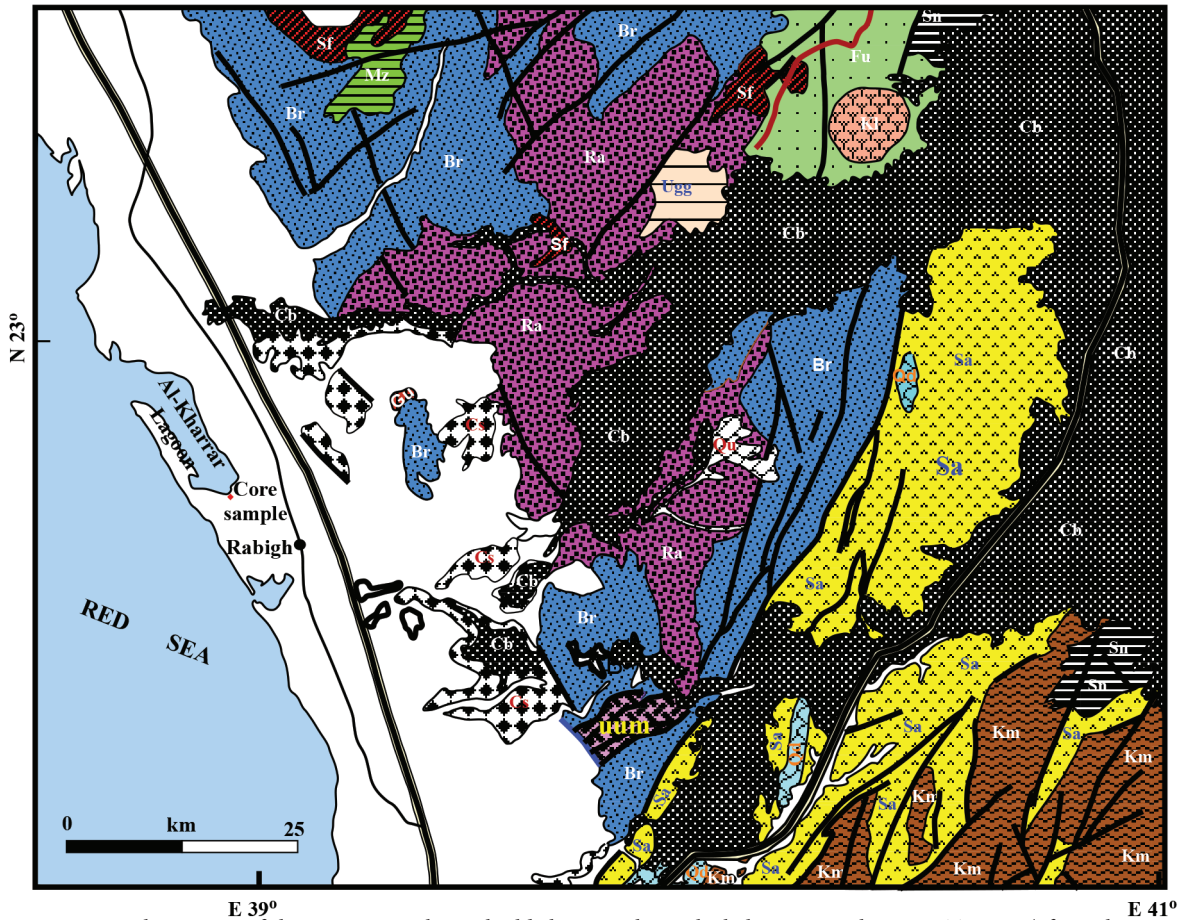

Figure 2. Geologic map of the western Arabian Shield showing the rocks belonging to the Hijaz Terrane (after Johnsson, 2006). Cs = Cenozoic sedimentary rocks, Cb = Cenozoic basalt, Br = Birak group, Sa = Samran group, Ra = Rabigh Suite, Km = Kamil Suite, Qd = Qudayd Suite, Sn = Shayma Nasir group, Kl = Kuhls granite, Sf = Subh Suite, Gu = Umm Gerad granite, Mz = Milhah Formation, Fu = Furayh group, Ugg = unassigned granite.

from 16% to 69% (average: 42%), whereas the ranges of silt and clay are 28%–79% and 3%–9%, respectively. The contact between the two facies is sharp, nonerosive, and remarkably distinguished by an abrupt color change. The regressive stacking pattern of the two facies is attributed to the late Holocene sea-level fall (Ghandour and Haredy, 2019). The present study is unique as it introduces for the first time detailed mineralogical and geochemical investigations for the late Holocene subsurface sediments along the Red Sea coast.

3. Materials and methods

A short sediment core (2.05 m long) was collected manually by pushing with rotation using a 6.35-cm PVC tube from the tidal flat south of Al-Kharrar Lagoon, North Rabigh area. The core was split into two halves, lithologically described and systematically subsampled at 4 cm apart. Fifty samples (37 for LG facies and 13 for TF facies) were dried at 50 °C and analyzed to determine the chemical and mineralogical composition. The mineralogical composition of 28 samples was determined using X-ray powder diffraction (XRD) (Shimadzu) with Ni-filtered Cu Kα radiation at 15 kV to 40 mA at the XRD laboratory of the Faculty of Marine Science, King Abdulaziz University. About 1 g of finely powdered sediments was packed into a cavity bearing an aluminum slide that was scanned at an interval from 2° to 60° 2θ scanning at speed of 1°/min. The relative abundance of the various minerals was determined semiquantitatively by measuring the height of the main reflections (Hardy and Tucker, 1988; Moore and Reynolds, 1989). The chemical composition of 50 samples was determined using the conventional XRF technique (Tawfik et al., 2017) at the Department of Geosciences, Osaka City University, Japan. The samples were completely dried and powdered using an agate mortar. Lithium tetraborate was mixed with the powdered samples and heated to 1000 °C to form a fused sample for X-ray fluorescence analysis. The analysis was carried out under 50 kV and 50 mA accelerating voltage

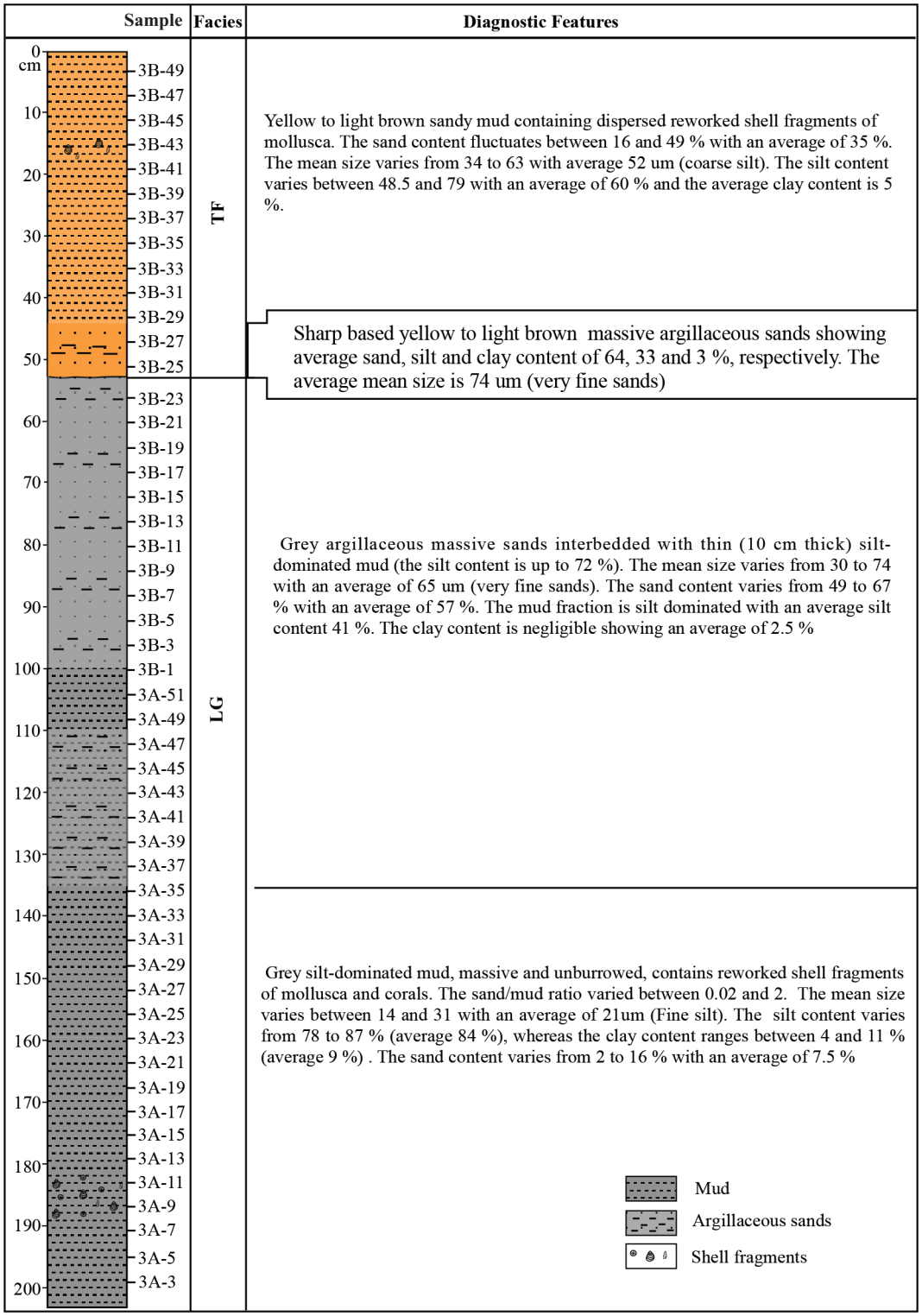

Figure 3. The sedimentary facies of the shallow subsurface sediments of the tidal flat south of Al-Kharrar Lagoon, Rabigh area (modified after Ghandour and Haredy, 2019).

and tube current, respectively, using a Rigaku RIX 2100 X-ray fluorescence spectrometer (XRF) equipped with an Rh/W dual-anode X-ray tube. In addition, 27 samples were analyzed to determine the organic carbon and $CaCO_3$ content using loss on ignition (LOI) at 550 °C (Heiri et al., 2001) and a calcimeter, respectively. Geochemical references, including the average chemical composition of the recent bottom sediments of the shallow nearshore area in the Al-Kharrar Lagoon (Basaham et al., 2015), different rocks of the Arabian-Nubian Shield east of Rabigh (Brown et al., 1989), the UCC (Taylor and McLennan, 1985), and rocks from different geotectonic settings (Bhatia, 1983) were selected for comparison. The shortcoming of the present study is the absence of a time framework for the sediments under investigation. However, the age of the sediment core (2.05 m long) in the present study is not older than 5500 years compared with a well-dated short sediment core (2.25 m long) collected from the NE part of the Al-Kharrar Lagoon (Bantan et al., 2019).

4. Results

The results of mineralogical and chemical analyses are summarized in Tables 1 and 2. To avoid the effect of dilution by organic matter and $CaCO_3$, the environmentally significant major and trace elements were normalized by Al (Calvert and Pedersen, 1993). The downcore variations of Al-normalized selected major and trace elements and the enrichment factors calculated for V, Cr, Cu, and Zn are shown in Figure 4 and the elemental ratios and paleoweathering indices employed in the present study are shown in Figure 5.

4.1. Mineralogy

XRD analysis showed the similar mineralogical composition of the two facies, except for limited vertical variations in the relative abundance of minerals (Table 1). The mineralogical composition is dominated by quartz, plagioclase, and K-feldspars with a moderate abundance of phyllosilicates, hornblende, and low Mg-calcite (LMC) and traces of mica, high Mg-calcite (HMC), dolomite, and gypsum (Table 1). Phyllosilicates and mica displayed relatively higher abundances in the sediments of lagoonal facies than those in intertidal flat facies, whereas the sediments of the intertidal flat facies yielded the highest quartz, plagioclase, and K-feldspar content. Although it is recorded with relatively low abundance, dolomite is relatively abundant in the upper part of the lagoonal facies and in the sediments of intertidal flat facies (Table 1). Gypsum is recorded generally with low abundances; however, a peak of gypsum (37%) was recorded from the middle part of the lagoonal facies.

4.2. Geochemistry

4.2.1. Major elements

The concentrations of SiO_2, Al_2O_3, Fe_2O_3, MnO, MgO, and K_2O exhibit slight variations between the two facies (Table 2). The concentration of SiO_2 increased slightly in the sediments of intertidal flat facies, whereas Al_2O_3, Fe_2O_3, MnO, MgO, and K_2O show reduced concentrations in the sediments of intertidal flat facies. The CaO, K_2O, and Na_2O display no remarkable variations in the two facies. SiO_2 displays a slight increase in concentration at the depth interval of 104–142 cm, with a decrease in the

Table 1. The results of mineralogical analysis using XRD for the shallow subsurface sediments of the tidal flat south of Al-Kharrar Lagoon. Phyl: Phyllosilicates, HMC: high Mg-calcite, LMC: low Mg-calcite.

Sample	Phyl %	Mica %	Amphiboles %	Gypsum %	Quartz %	Plagiocl ase%	K- Feldspars %	HMC %	LMC %	Dolomite %
3B-41	9	3	3	0	44	20	14	3	3	0
3B-39	8	3	3	2	35	18	20	4	6	3
3B-37	6	3	9	1	32	27	6	3	10	2
3B-35	8	4	6	0	47	22	7	0	4	3
3B-33	7	2	3	0	43	31	9	0	3	2
3B-31	5	1	5	0	61	13	6	3	5	2
3B-29	6	2	8	0	49	23	5	3	2	2
3B-27	7	2	5	0	36	21	18	5	2	3
3B-25	8	3	5	0	48	21	8	3	3	2
3B-23	12	4	3	4	35	17	7	11	5	3
3B-21	10	3	7	0	44	16	9	3	5	3
3B-19	11	4	3	2	45	32	0	0	4	0
3B-17	12	5	5	0	39	20	11	0	5	3
3B-15	8	2	2	0	32	14	35	2	3	2
3B-13	12	4	5	0	48	16	0	4	4	7
3B-9	9	3	5	0	47	21	8	0	4	3
3B-7	6	3	4	0	55	17	9	3	2	2
3B-5	5	1	2	4	27	56	4	0	1	0
3B-1	4	1	4	37	35	11	5	0	1	1
3A-51	23	0	9	0	33	21	0	6	8	0
3A-43	15	7	0	11	30	17	7	5	8	0
3A-39	14	9	9	0	34	9	19	0	6	0
3A-35	11	0	0	0	41	19	13	9	8	0
3A-29	20	7	0	0	43	23	0	7	0	0
3A-21	19	6	0	0	27	13	26	5	5	0
3A-15	18	9	6	0	36	14	7	0	9	0
3A-9	23	10	8	0	31	12	7	0	10	0
3A-3	16	5	11	0	33	14	15	0	5	0

Table 2. Summary of geochemical results, elemental ratios, paleoweathering indices (CIA, PIA, CIW, and ICV), and enrichment factors of the redox-sensitive trace elements of the shallow subsurface sediments of the tidal flat south of Al-Kharrar Lagoon (abbreviations are explained in the text).

Element	Lagoonal facies (LG)			Tidal flat facies (TF)			I	II	III	IV	UCC	OIA	CIA	AM	PM
	Min	Max	mean	Min	Max	mean									
SiO_2 %	52.21	57.77	54.85	57.77	61.87	59.36	52.54	62.1	46.7	72.6	66.6	58.83	70.69	73.86	81.95
TiO_2 %	1.03	1.57	1.16	0.97	1.16	1.09	1.08	1.4	0.16	0.22	0.64	1.06	0.64	0.46	0.49
Al_2O_3 %	14.57	18.09	16.23	14.96	15.65	15.32	15.885	14	20.7	14.9	15.4	17.11	14.04	12.89	8.41
Fe_2O_3 %	7.94	9.69	8.74	6.66	7.74	7.39	8.83	7.5	7.6	2.2	5.04	8.08	4.82	3.06	3.28
MnO %	0.13	0.17	0.14	0.11	0.13	0.12	0.125	0.15	0.1	0.01	0.1	0.15	0.1	0.1	0.05
MgO %	4.58	6.67	5.35	3.75	4.51	4.23	5.75	1.5	9.4	0.42	2.48	3.65	1.97	1.23	1.39
CaO %	3.83	6.48	5.07	4.55	5.25	4.97	7.3	4.1	12.6	1.8	3.59	5.83	2.68	2.48	1.89
Na_2O %	3.99	5.45	4.56	3.94	6.13	4.51	2.5	5.4	1.7	3.6	3.27	4.1	3.12	2.77	1.07
K_2O %	1.4	1.98	1.63	1.25	1.54	1.46	1.515	0.97	0.2	4.1	2.8	1.6	1.89	2.9	1.71
V (µg/g)	250	350	277	230	273	257									
Cr (µg/g)	154	236	176	141	172	161									
Cu (µg/g)	38	75	56	16	49	40									
Zn (µg/g)	54	90	69	40	71	60									
Rb (µg/g)	34	53	42	23	39	35									
Sr (µg/g)	239	419	314	325	346	337									
Zr (µg/g)	158	347	196	156	198	183									
Ce (µg/g)	8	26	18	13	22	16									
Nd (µg/g)	14	21	18	15	20	18									
$CaCO_3$ %	0.00	4.28	1.63	0.73	1.92	0.89									
C_{org} %	1.33	9.03	4.94	1.32	5.59	3.75									
Al_2O_3/TiO_2	9.4	17	14	13	15	14									
Al/Si	0.29	0.39	0.34	0.28	0.3	0.29									
V/Cr	1.43	1.71	1.58	1.56	1.68	1.6									
Cu/Zn	0.59	1.01	0.82	0.41	0.74	0.65									
K/Rb	296	371	323	328	461	353									
CIA	44	52	47	42	48	46									
PIA	43	52	47	42	47	46									
CIW	46	55	49	44	50	48									
ICV	1.51	1.93	1.65	1.45	1.66	1.6									
EF_V	1.92	2.69	2.13	1.77	2.10	1.98									
EF_{Cr}	1.71	2.62	1.95	1.57	1.91	1.79									
EF_{Cu}	0.85	1.66	1.25	0.36	1.09	0.88									
EF_{Zn}	0.57	0.95	0.72	0.42	0.75	0.64									

I = Average chemical composition of shallow sediments of Al-Kharar Lagoon (Basaham et al., 2015); II–IV = the chemical composition of Na-dacite, diorite, and granodiorites, respectively (samples 102, 104, and 105, respectively; Brown et al., 1989). UCC: Taylor and McLennan (1985). OIA, CIA, AM, and PM are oceanic island arc, continental island arc, active margin, and passive margin, respectively (Bhatia, 1983).

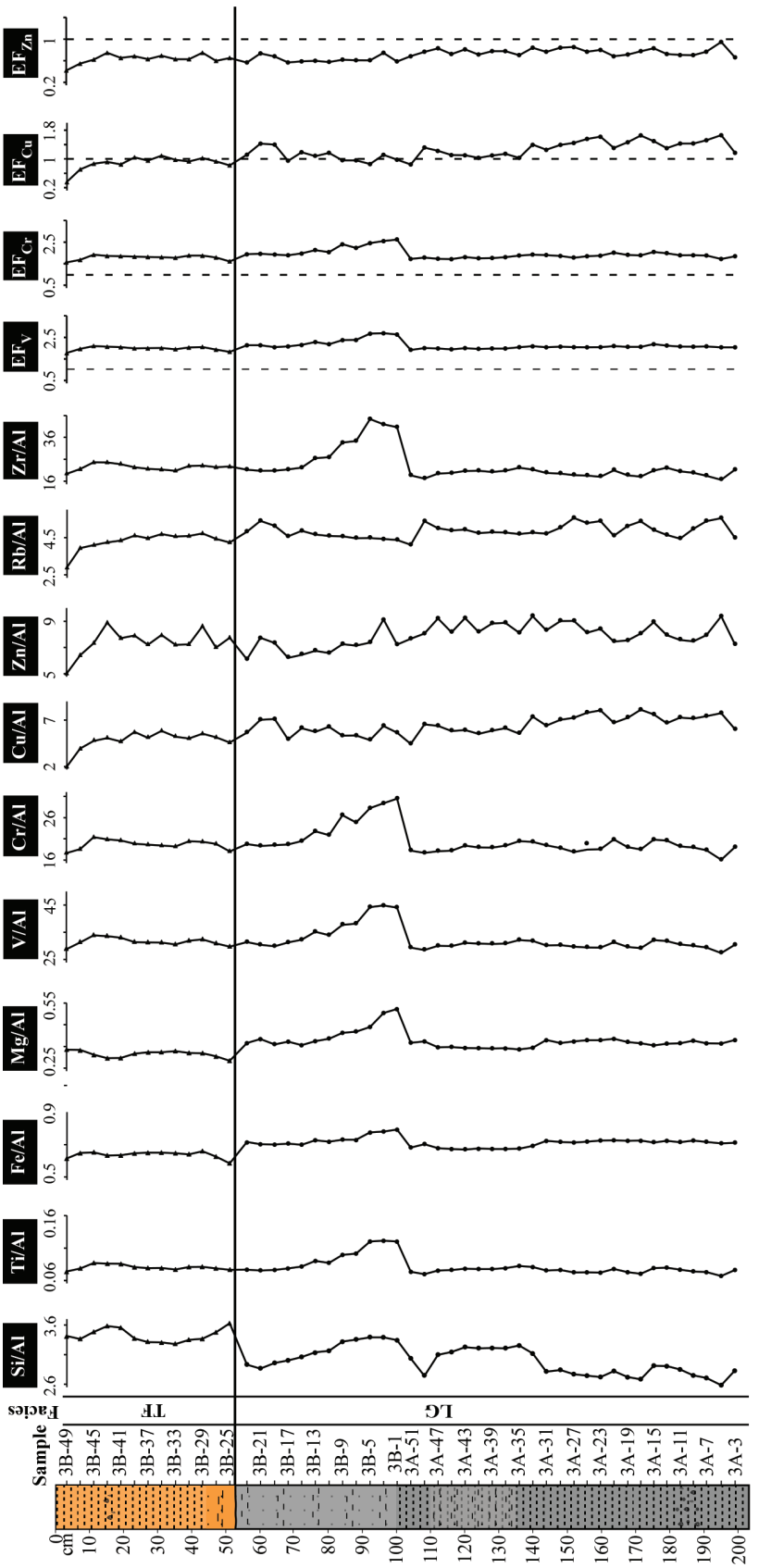

Figure 4. Downcore trends of the Al-normalized selected major (Si, Ti, Fe, and Mg) and trace (V, Cr, Cu, Zn, Rb, and Zr) elements and enrichment factor for redox sensitive trace elements (V, Cr, Cu, and Zn).

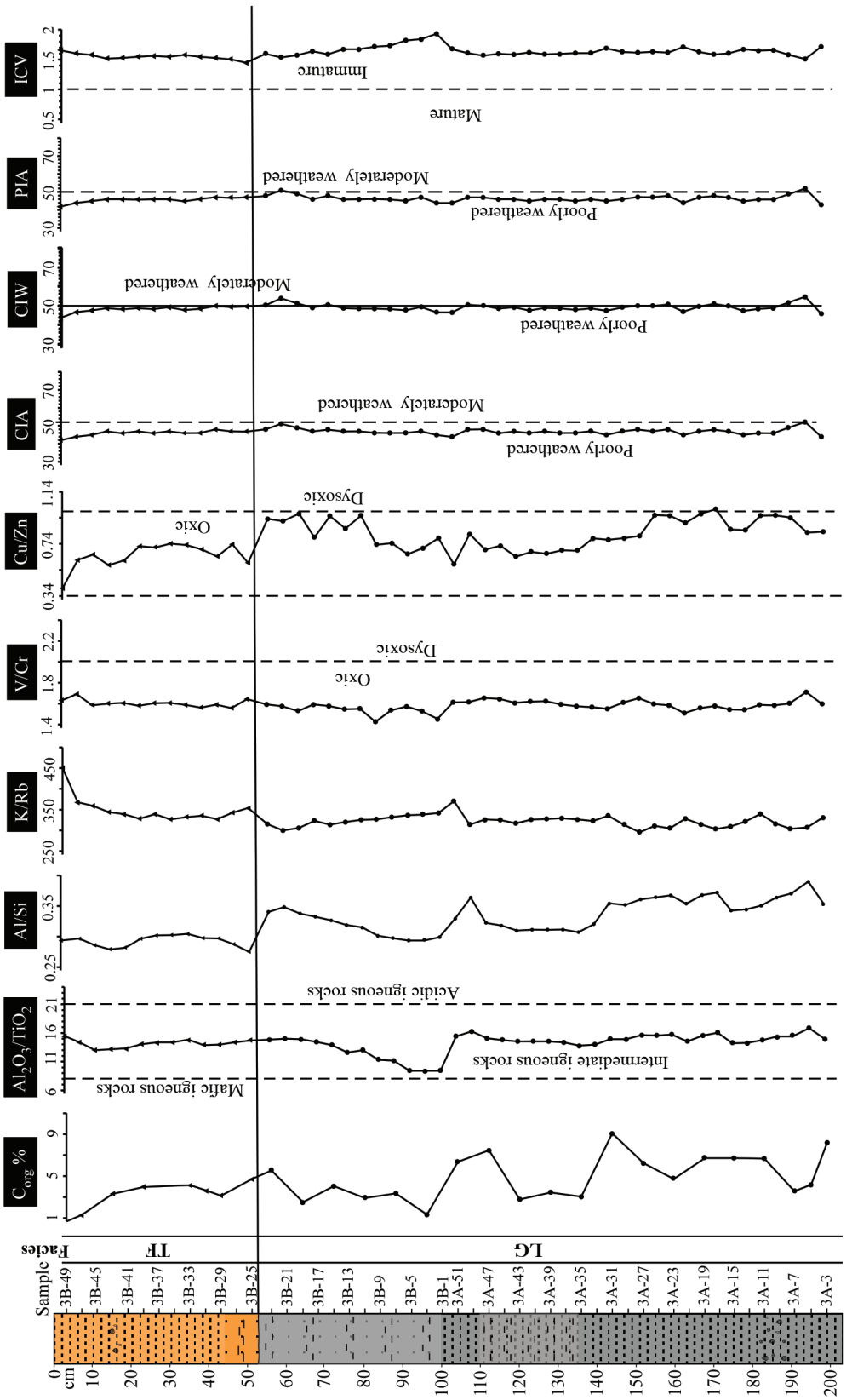

Figure 5. Downcore variations of organic carbon, elemental ratios (Al2O3/TiO2, Al/Si, K/Rb, V/Cr, and Cu/Zn), and indices for paleoweathering (CIA, CIW, and PIA) and compositional maturity (ICV).

concentrations of Al_2O_3, Fe_2O_3, MnO, and MgO. SiO_2 varies between 52.21% and 57.77% with an average of 54.85% in the sediments of facies LG, whereas it varies in the sediments of facies TF from 57.77% to 61.87% with an average of 59.36%. The average concentrations of Al_2O_3, Fe_2O_3, MgO, and MnO in the sediments of facies LG are 16.231%, 8.74%, 5.35%, and 0.144%, respectively, whereas their concentrations in the sediments of facies TF are 15 ± 0.25%, 7.39 ± 0.32%, 4.23 ± 0.25%, and 0.12 ± 0.01%, respectively (Table 2).

The Si/Al ratios in the sediments of the TF facies are higher than their counterparts in the LG facies. The Al-normalized Ti, Fe, and Mg show no remarkable variations between the sediments of the two facies. However, peaks of increased Ti/Al, Fe/Al, and Mg/Al ratios are observed at a depth of 90–105 cm (Figure 4).

The average concentrations of major elements in the two facies are normalized (Figures 6a–6i) relative to the average chemical composition of nearshore recent bottom sediments of the Al-Kharrar Lagoon (Basaham et al., 2015); of igneous rocks' dacite, diorite, and granodiorite of the Arabian Shield east of Rabigh (samples 102, 104, and 105, respectively; Brown et al., 1989); of UCC (Taylor and McLennan, 1985); and of rocks from different tectonic settings (Bhatia, 1983). The normalization showed that the subsurface sediments of the tidal flat south of Al-Kharrar Lagoon are closely correlated, except for a slight deviation of some elements with the average chemical composition of recent sediments, dacite, diorite, and rocks of oceanic island arc (Figures 6a–6c and 6f). Compared to the recent sediments, dacite, diorite, and oceanic island arc rocks, CaO is slightly depleted, whereas SiO_2, TiO_2, Al_2O_3, Fe_2O_3, and MnO show a similar order of concentrations. On the other hand, Na_2O is enriched relative to the average recent sediments of the Al-Kharrar Lagoon, and K_2O and MgO are enriched relative to dacite, diorite, and OIA.

4.2.2. Trace elements

The behavior of trace elements does not change remarkably between the two facies (Table 2). However, trace elements V, Cr, Zr, Ce, and Nd show an abrupt increase in depths of 90–105 cm from the top. The concentrations of V, Cr, Cu, Zn, Rb, and Zr in the sediments of facies LG are 250–350 µg/g, 154–236 µg/g, 38–75 µg/g, 54–90 µg/g, and 158–347 µg/g, respectively (Table 2). The average concentrations of the same elements in the sediments of facies TF were 257, 161, 40, 60, 35, and 183 µg/g, respectively (Table 2). These elements display a similar distribution pattern, implying their possible similar source. The downcore profiles of the Al-normalized V, Cr, Cu, Zn, Rb, and Zr appear to be constant, except for a peak of increased V/Al, Cr/Al, and Zr/Al at depths of 90–105 cm (Figure 5).

The elemental relationships show a poor to a negative correlation between the SiO_2 and major oxides, suggesting that SiO_2 is strongly associated with quartz (Tables 3 and 4). Al_2O_3 shows a strong positive correlation with Fe_2O_3, K_2O, Cu, and Rb, suggesting an association with clay minerals. The CaO correlates positively with Sr, indicating that Sr is linked to carbonate minerals. TiO_2 is strongly correlated with V, Cr, and Zr, indicating that these elements are associated with heavy minerals.

4.2.3. Enrichment factor

The enrichment factor (EF) for the environmentally significant trace elements (V, Cr, Cu, and Zn) is determined as the ratio of the element relative to the same element in a reference material (Liu et al., 2012). The reference material is selected as the average shale composition (Li and Schoonmaker, 2010). EF values of >1 indicate enrichment, values of <1 indicate depletion, and values equal to 1 indicate no enrichment/depletion. The EF values show that V and Cr are generally >1 in the sediments of both lagoonal and intertidal flat facies, indicating enrichment relative to the average shale. The EF values for V and Cr are in the ranges of 1.92–2.69 and 1.71–2.62, respectively, for the sediments of the LG facies and 1.77–2.1 and 1.57–1.9, respectively, for the sediments of the TF facies (Table 2). On the other hand, the average EF values of Cu for the sediments of the LG and TF facies are 1.25 and 0.88, respectively. The EF values of Zn are generally <1 (Table 2) in the sediments of the LG and TF facies, suggesting depletion relative to the average shale (Figure 4).

4.2.4. Organic and inorganic carbon content

The calcium carbonate content in the sediments of facies LG varies between 0% and 4% with an average of 2%, whereas it varies in the sediments of facies TF from 1 to 2 with an average of 1% (Table 2). The basal part of facies LG contains the highest $CaCO_3$ content and the values decrease upward. The sediments of facies LG yield relatively higher organic carbon contents compared to the sediments of the intertidal flat facies (Figure 5). The organic carbon content varies in the sediments of facies LG from 1.3% to 9% with an average of 4.96% and from 1.32% to 4.76% with average of 3.5% in the sediments of facies TF (Table 2).

4.3. Provenance and tectonic setting

The geochemical classification of the sediments using variable plots (Pettijohn et al., 1972; Blatt et al., 1980; Lindsey, 1999) indicates greywacke (Figures 7a–7c).

Several geochemical proxies have been employed to characterize sediment provenance. These proxies include the discriminant functions (Roser and Korsch, 1986), the ratios of immobile elements (Al_2O_3/TiO_2; Hayashi et al., 1997), and Zr (µg/g) vs. TiO_2 % and K_2O % vs. Rb (µg/g) biplots. In the provenance discrimination diagram of Roser and Korsch (1988), the discriminant functions depend on the concentrations of mobile to immobile major elements. On the discriminant function diagram, the

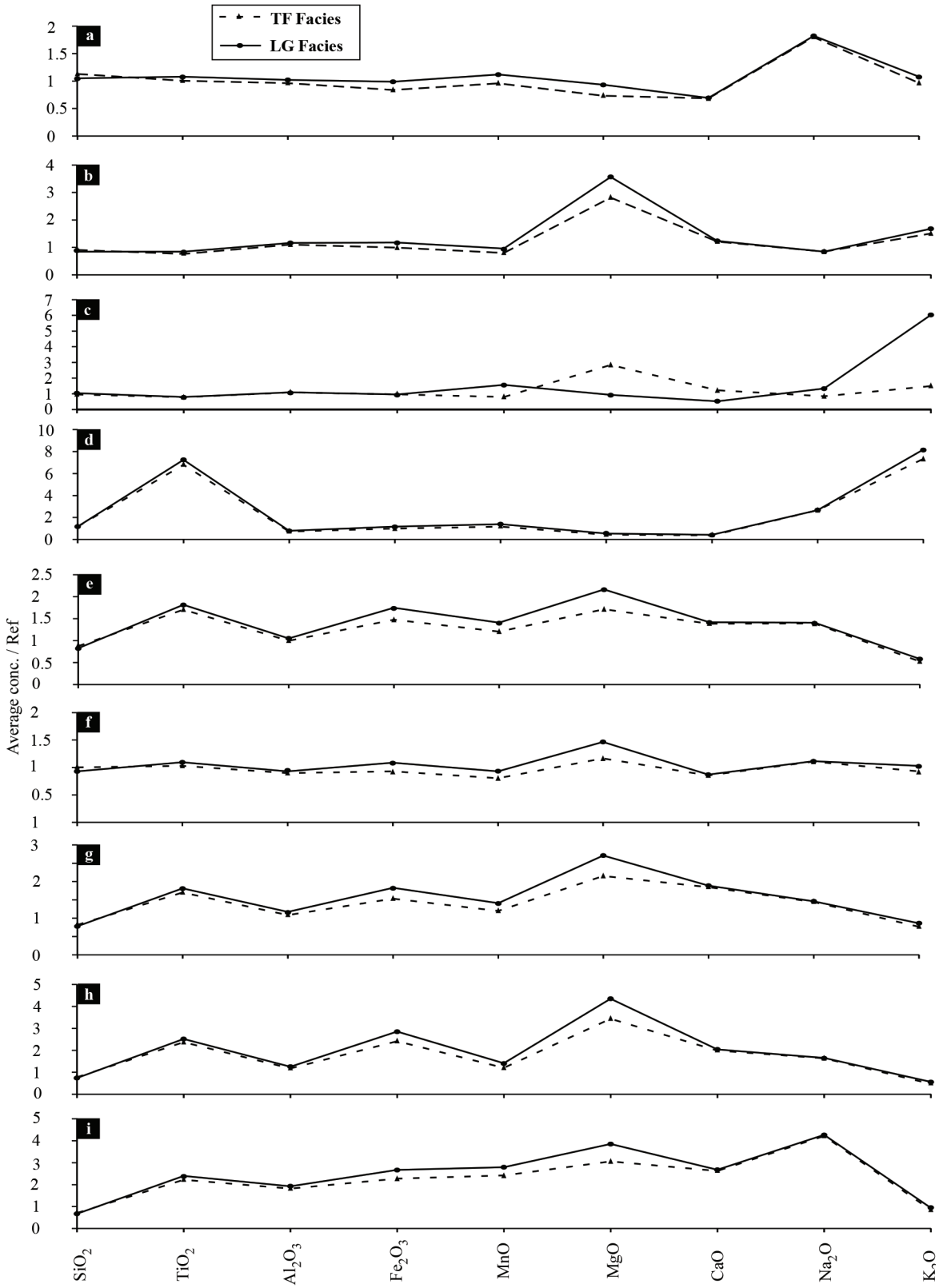

Figure 6. Normalization of the average concentrations of major elements (wt.%) in the sediments of the lagoonal (LG) and tidal flat (TF) facies against a) average chemical composition of shallow bottom sediments of Al-Kharrar Lagoon (Basaham et al., 2015); b–d) the chemical composition of Na-dacite, diorite, and granodiorites, respectively (samples 102, 104, and 105, respectively; Brown et al., 1989); e) upper continental crust (Taylor and McLennan, 1985); and f–i) average chemical composition of sediments from different tectonic settings, OIA, CIA, AM, and PM, respectively (Bhatia, 1983).

Table 3. Elemental interrelationships of the lagoonal facies sediments (n = 37).

	SiO_2	TiO_2	Al_2O_3	Fe_2O_3	MnO	MgO	CaO	Na_2O	K_2O	V	Cr	Cu	Zn	Rb	Sr	Zr	Ce	Nd
SiO_2																		
TiO_2	0.38																	
Al_2O_3	–0.73	–0.71																
Fe_2O_3	–0.84	–0.10	0.74															
MnO	–0.16	0.39	–0.06	0.36														
MgO	–0.39	0.60	–0.01	0.60	0.51													
CaO	–0.33	–0.13	–0.09	–0.02	–0.05	–0.15												
Na_2O	–0.23	–0.38	0.21	0.01	0.04	–0.10	–0.21											
K_2O	–0.66	–0.66	0.94	0.67	–0.15	0.03	–0.27	0.26										
V	0.29	0.99	–0.62	0.03	0.44	0.67	–0.14	–0.39	–0.58									
Cr	0.28	0.96	–0.64	0.01	0.49	0.65	–0.04	–0.42	–0.63	0.97								
Cu	–0.69	–0.46	0.84	0.76	–0.08	0.16	–0.01	–0.19	0.83	–0.36	–0.37							
Zn	–0.29	–0.44	0.50	0.23	–0.42	–0.14	–0.10	–0.11	0.65	–0.42	–0.48	0.64						
Rb	–0.58	–0.59	0.91	0.67	–0.10	0.04	–0.32	0.11	0.97	–0.50	–0.54	0.86	0.60					
Sr	0.06	0.35	–0.53	–0.27	0.03	0.05	0.81	–0.35	–0.68	0.30	0.37	–0.40	–0.38	–0.70				
Zr	0.41	0.99	–0.74	–0.15	0.41	0.57	–0.11	–0.35	–0.69	0.97	0.95	–0.51	–0.49	–0.62	0.37			
Ce	–0.32	0.42	0.17	0.63	0.56	0.62	–0.06	–0.26	0.05	0.51	0.48	0.24	–0.26	0.14	0.00	0.41		
Nd	–0.14	0.48	–0.06	0.34	0.18	0.62	–0.17	–0.23	0.00	0.53	0.48	0.10	0.02	0.05	0.04	0.47	0.36	

Table 4. Elemental interrelationships of the tidal flat facies sediments (n = 13).

	SiO_2	TiO_2	Al_2O_3	Fe_2O_3	MnO	MgO	CaO	Na2O	K2O	V	Cr	Cu	Zn	Rb	Sr	Zr	Ce	Nd
SiO_2																		
TiO_2	0.29																	
Al_2O_3	–0.52	0.17																
Fe_2O_3	–0.59	0.49	0.84															
MnO	–0.80	–0.41	0.08	0.26														
MgO	–0.98	–0.20	0.68	0.71	0.71													
CaO	–0.37	0.48	–0.01	0.41	0.41	0.33												
Na_2O	–0.63	–0.75	–0.21	–0.24	0.68	0.48	0.10											
K_2O	0.00	0.44	0.84	0.66	–0.36	0.21	–0.23	–0.67										
V	0.13	0.98	0.30	0.63	–0.30	–0.03	0.52	–0.72	0.51									
Cr	0.11	0.94	0.38	0.64	–0.40	–0.01	0.36	–0.68	0.58	0.95								
Cu	0.16	0.62	0.70	0.62	–0.44	0.03	–0.11	–0.81	0.93	0.65	0.70							
Zn	0.46	0.69	0.36	0.37	–0.56	–0.29	–0.06	–0.93	0.70	0.68	0.67	0.85						
Rb	0.12	0.57	0.76	0.64	–0.45	0.08	–0.17	–0.77	0.98	0.61	0.67	0.98	0.81					
Sr	0.03	0.24	–0.27	–0.07	0.00	–0.06	0.66	0.05	–0.32	0.24	0.12	–0.25	–0.05	–0.28				
Zr	0.60	0.91	–0.01	0.20	–0.64	–0.50	0.17	–0.88	0.43	0.85	0.82	0.59	0.76	0.55	0.17			
Ce	–0.09	0.37	0.11	0.39	0.14	0.13	0.13	–0.27	0.21	0.45	0.36	0.13	0.24	0.19	–0.22	0.38		
Nd	–0.34	0.51	0.56	0.73	0.24	0.41	0.49	–0.30	0.48	0.59	0.52	0.53	0.34	0.49	0.15	0.28	0.14	

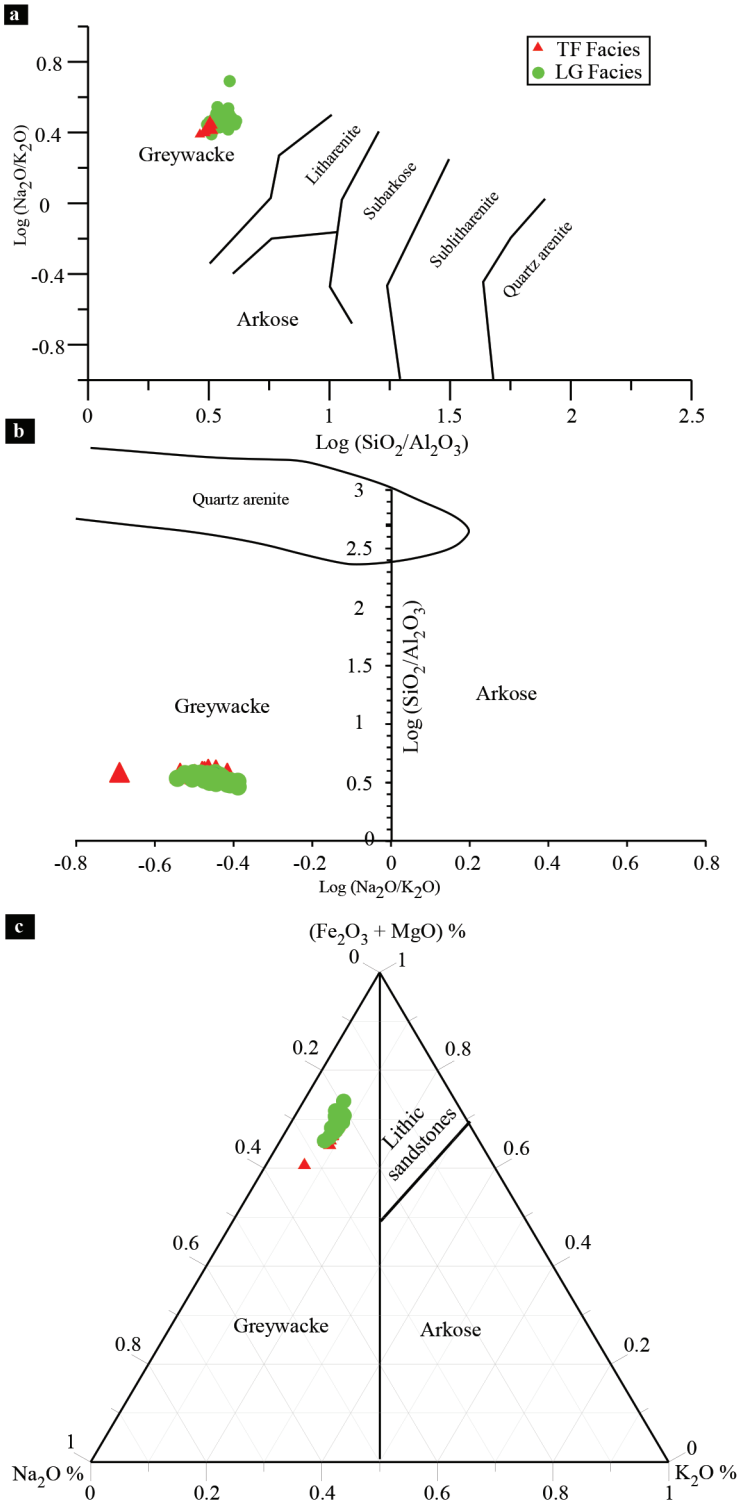

Figure 7. Geochemical classification of the sediments in the present study after a) Pettijohn et al. (1972), b) Blatt et al. (1980), and c) Lindsey (1999).

sediments are mostly plotted in the field of intermediate igneous provenances (Figure 8a). The Al_2O_3/TiO_2 ratio varies in mafic rocks from 3 to 8, in intermediate rocks from 8 to 21, and in acidic igneous rocks from 21 to 70 (Hayashi et al., 1997). The Al_2O_3/TiO_2 ratio (Table 2) for the sediments of the TF facies varies between 13 and 15.4

(average: 14.14) and in the sediments of the LG facies from 9.4 and 17 (average: 14.2). These values suggest that the sediments were derived predominantly from intermediate igneous source rocks (Figures 5 and 8b). The bivariate plot of Zr (μg/g) vs. TiO_2 % has been employed to interpret the source rock composition (Chen et al., 2017). This plot (Figure 8c) shows that the sediments of the two facies were derived from intermediate andesitic source rock. Similarly, the bivariate plot of K_2O % vs. Rb (μg/g) (Floyd and Leveridge, 1987) shows that the sediments were derived from a generally uniform and chemically coherent intermediate source rock (Figure 8d).

The tectonic setting of the source area is best identified using 1) the bivariate plot between K_2O/Na_2O and SiO_2/Al_2O_3 on a log scale, 2) the discriminant function (Roser and Korsch, 1988), and 3) the discriminant function using (Fe_2O_3+Mgo) % vs. Al_2O_3/SiO_2 and TiO_2 % (Bhatia, 1983). The biplot of SiO_2 % versus K_2O/Na_2O (Roser and Korsch, 1986) has been adopted to interpret the tectonic setting of the source area. The sediments are plotted in the oceanic island arc tectonic (OIA) setting (Figure 9a). On the bivariate plot of K_2O/Na_2O vs. SiO_2/Al_2O_3, the samples are clustered in the A1 field, suggesting OIA (Figure 9b). The compositionally immature sediments are consistent with OIA and intermediate composition.

5. Discussion

The siliciclastic-dominated shallow subsurface sediments of the tidal flat south of Al-Kharrar Lagoon contain two sedimentary facies: gray mud and argillaceous sand of lagoonal origin, sharply overlain by brown mud and argillaceous sands of intertidal flat origin. Mineralogical composition shows a dominantly detrital origin with occasional occurrence of low abundant carbonate and evaporite minerals. The occasional occurrence of gypsum is explained by the evaporative pumping mechanism of shallow groundwater. Lenticular gypsum crystals grow diagenetically in the pore spaces of siliciclastic sediments by displacive growth from the fluctuating groundwater (Aref et al., 1997; Aref and Taj, 2018). The chemical composition of the sediments is fundamentally controlled by the source rock composition and secondarily by hydraulic sorting. The redox conditions of the Al-Kharrar paleolagoon bottom played no role in the enrichment of trace elements.

5.1. Sediment source

The sediments of the two facies are first-cycle geochemically and mineralogically immature greywacke derived mainly from a source rock of intermediate igneous rocks that did not change over time. However, increasing mafic input is observed at depths of 90 to 105 cm from the top by the slight enrichment of V and Cr. The igneous and metamorphic rocks belonging to the Hijaz Terrane are expected to be the source of the sediments. The rocks that make up the Hijaz Terrane include assemblages of calc-alkaline volcanic and intrusive igneous rocks such as basalt, andesite, diorite, tonalite, and granodiorites mostly developed as magmatic arcs at convergent boundaries.

To the east of Rabigh city, the Birak (volcanic complex) group is discontinuously exposed along the southern margin of the Hijaz Terrane, consisting mainly of metamorphosed low K-tholeiitic volcanic and volcaniclastic sedimentary rocks of intraoceanic origin. The rock types of the Birak group include green-schist-facies basaltic, andesitic, dacitic, diorite, rhyolitic flows, pyroclastic rocks (agglomerate, lapilli tuff, and ash tuff), greywacke, marble, quartzite, and chert (Ramsay, 1986; Johnson et al., 2003; Hargrove et al., 2006; Johnson, 2006). Island-arc remnants are very common in the western Arabian Shield and they form the core of the main terranes (Brown et al., 1989). The Hijaz island arc would have collided on the Jiddah Terrane after its back-arc basin or fore-arc had been subducted at the Jiddah island arc and the Bi'r Umq ophiolite was therefore a part of the back-arc or the fore-arc of the Hijaz island arc (Hargrove et al., 2006; Johnson, 2006).

5.2. Paleoweathering

The intensity of weathering in clastic sediments in the source area can be evaluated by examining the relationships between alkali and alkaline earth elements (Nesbitt et al., 1997). Under the condition of intense chemical weathering, alkali and alkaline earth elements are readily mobilized. The paleoweathering conditions of sediments and sedimentary rocks can be evaluated using different indices, including the chemical index of alteration (CIA; Nesbitt and Young, 1982), the chemical index of weathering (CIW; Harnois, 1988), the plagioclase index of alteration (PIA; Fedo et al., 1995), and the index of compositional variations (ICV; Cox et al., 1995). In addition, the ratios between elements with different mobilities can be used to quantify the change in chemical weathering (McLennan, 1993).

CIA measures the degree of alteration of feldspars to clay minerals during weathering processes. It can be calculated using the equation $100 \times [A1_2O_3/(A1_2O_3 + CaO + Na_2O + K_2O)]$. CIA values of less than 51 indicate an unweathered or poorly weathered source, suggesting direct input from unweathered first-cycle intermediate source rock (McLennan, 1993). In sedimentary rocks, the increase in CIA value indicates advanced weathering of the source rocks. The CIA values are generally less than or slightly higher than 51 (Table 2; Figure 5). The CIA values in the sediments of facies LG varied between 44 and 51 (average: 47), while they varied from 42 to 48 with an average of 46 in the sediments of the intertidal flat facies (TF) (Table 2; Figure 5).

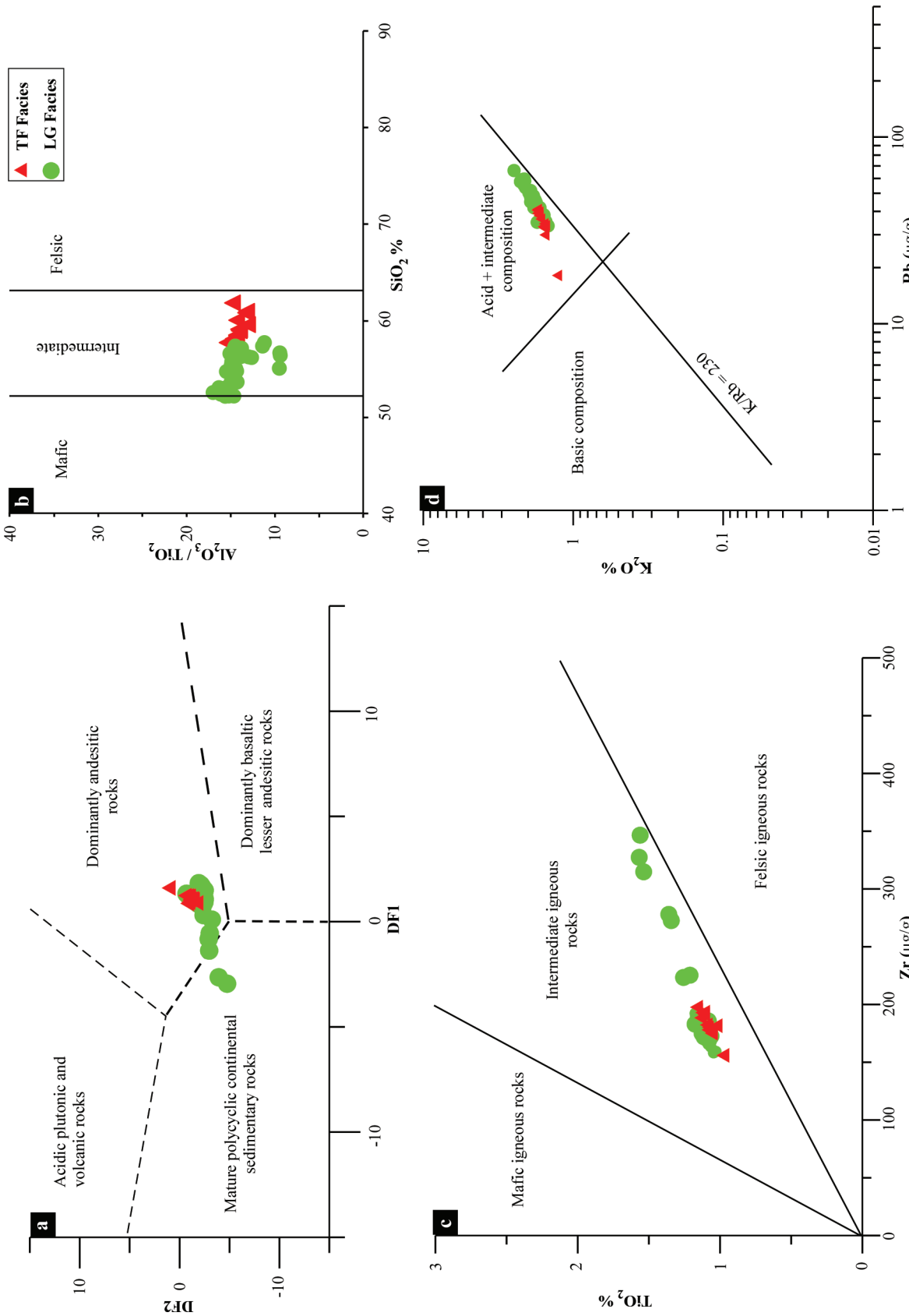

Figure 8. Discrimination diagrams for identifying the source rock composition of the shallow subsurface sediments at the tidal flat, south Al-Kharrar Lagoon. a) Discriminant diagram after Roser and Korsch (1988); b and c) biplots of SiO_2(%) vs. Al_2O_3/TiO_2 and Zr (µg/g) vs. TiO_2 % (after Hayashi et al., 1997); d) Rb-K_2O biplot (after Floyd and Leveridge, 1987).

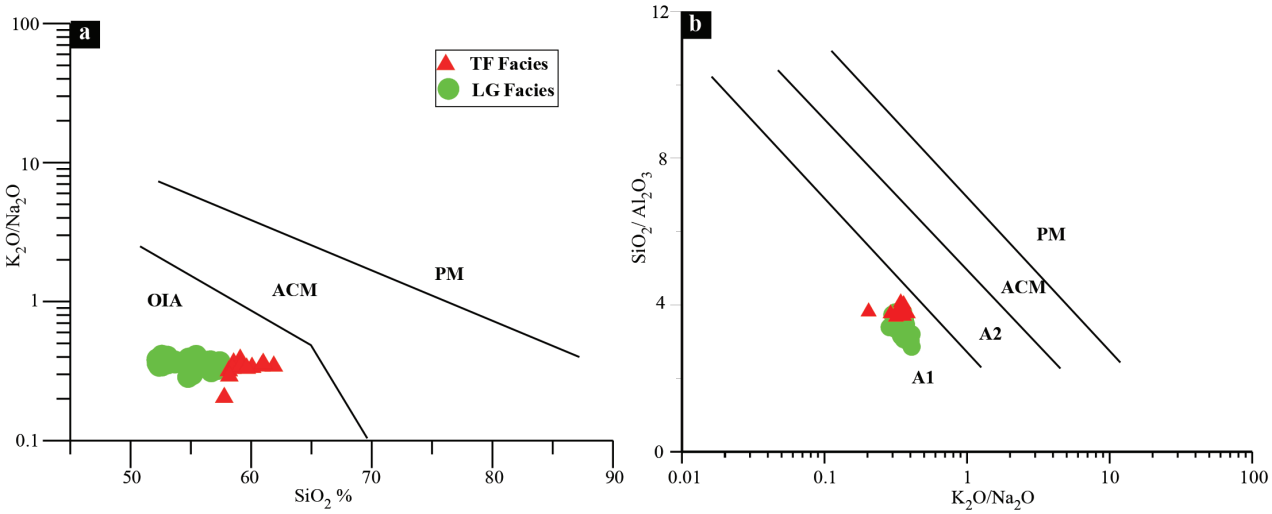

Figure 9. Discrimination diagrams for identifying the tectonic setting of the shallow subsurface sediments at the tidal flat, south Al-Kharrar Lagoon, Rabigh area. a) SiO_2 (%) vs. log (K_2O/Na_2O) for the investigated Holocene sediments (after Roser and Korsch, 1986); b) K_2O/Na_2O vs. SiO_2/Al_2O_3 diagram after Roser and Korsch (1986). OIA: Oceanic island arc, ACM: active continental margin, PM: passive margin, CIA: continental island arc, A1: arc setting (basaltic and andesitic detritus), A2: evolved arc setting, felsic-plutonic detritus.

CIW, calculated as [$Al_2O_3/(Al_2O_3 + CaO + Na_2O)$] × 100] (molecular proportion), was proposed to monitor paleoweathering at the source area, which is not sensitive to postdepositional K enrichments (Harnois, 1988). The CIW value increases as the degree of weathering increases. CIW values of less than 50 indicate unweathered rock. The sediments of the lagoonal facies have CIW values ranging from 46 to 55 with an average of 49, whereas the CIW of the intertidal flat facies ranged between 44 and 50 with an average of 48 (Table 2; Figure 5). The relatively low CIW values indicated that CaO and Na_2O are not leached because of a low degree of weathering.

PIA provides a proxy to determine the intensity of chemical weathering. It is calculated using the equation PIA = 100 × [(Al_2O_3 – K_2O/(Al_2O_3 + CaO + Na_2O - K_2O)]. PIA values of less than 50 indicate unweathered source rock. In the present study, the sediments of the lagoonal facies have PIA values varying between 41 and 48 with an average of 44, whereas the PIA values in the sediments of the intertidal flat facies ranged from 40 to 45 with an average of 43 (Table 2; Figure 5). These low values suggest unweathered to poorly weathered source rock.

ICV is used to measure compositional maturity (Cox et al., 1995; Potter et al. 2005). It is determined using the weight percentages of major oxides as follows: ICV = (CaO + K_2O + Na_2O + $Fe_2O_3^t$ + MgO + MnO + TiO_2)/ Al_2O_3, where $Fe_2O_3^t$ represents total iron and CaO represents all sources of Ca. ICV values of <1 indicate compositionally mature sediments, whereas ICV values of >1 indicate compositionally immature sediments. In the present study, the values of ICV are generally >1. The ICV values for the sediments of facies LG (1.51–1.93) are slightly higher than the ICV values for the sediments of facies TF (1.45–1.66), suggesting compositionally immature sediments, and these sediments are possibly first-cycle, probably derived from poorly weathered source rock (Table 2; Figure 5). The poor weathering is consistent with the arid climate. Compositionally immature sediments are common under poorly weathered source rock, whereas intensive weathering produces compositionally mature sediments.

The Al_2O_3-(CaO+Na_2O)-K_2O (A-CN-K) and Al_2O_3-(CaO+Na_2O+K_2O)-(Fe_2O_3+MgO) (A-CNK-FM) ternary diagrams (Figures 10a and 10b) introduced by Nesbitt and Young (1984, 1989) are used to interpret the degree of weathering. On the A-CN-K diagram (Figure 10a), the sediments derived from severely weathered sources plot high in the diagram near the A-apex with high CIA values (80–100), whereas those from unweathered to moderately weathered sources plot adjacent to the feldspar join with CIA values of 40–70 (Nesbitt and Young, 1996). The samples in the present study plot below but very close to the feldspar join with CIA values of 42% to 52% Al_2O_3, almost parallel to the A-CN side, suggesting unweathered to poorly weathered source rock (Figure 10a). Similarly, on the A-CNK-FM diagram, the sediments of the two facies fall below the line joining feldspar to the FM apex, suggesting a similar source rock composition of poorly weathered source rock similar to the original composition of fresh diorite (Figure 10b). The sediments contain relatively low clay mineral content and relatively high content of ferromagnesian minerals.

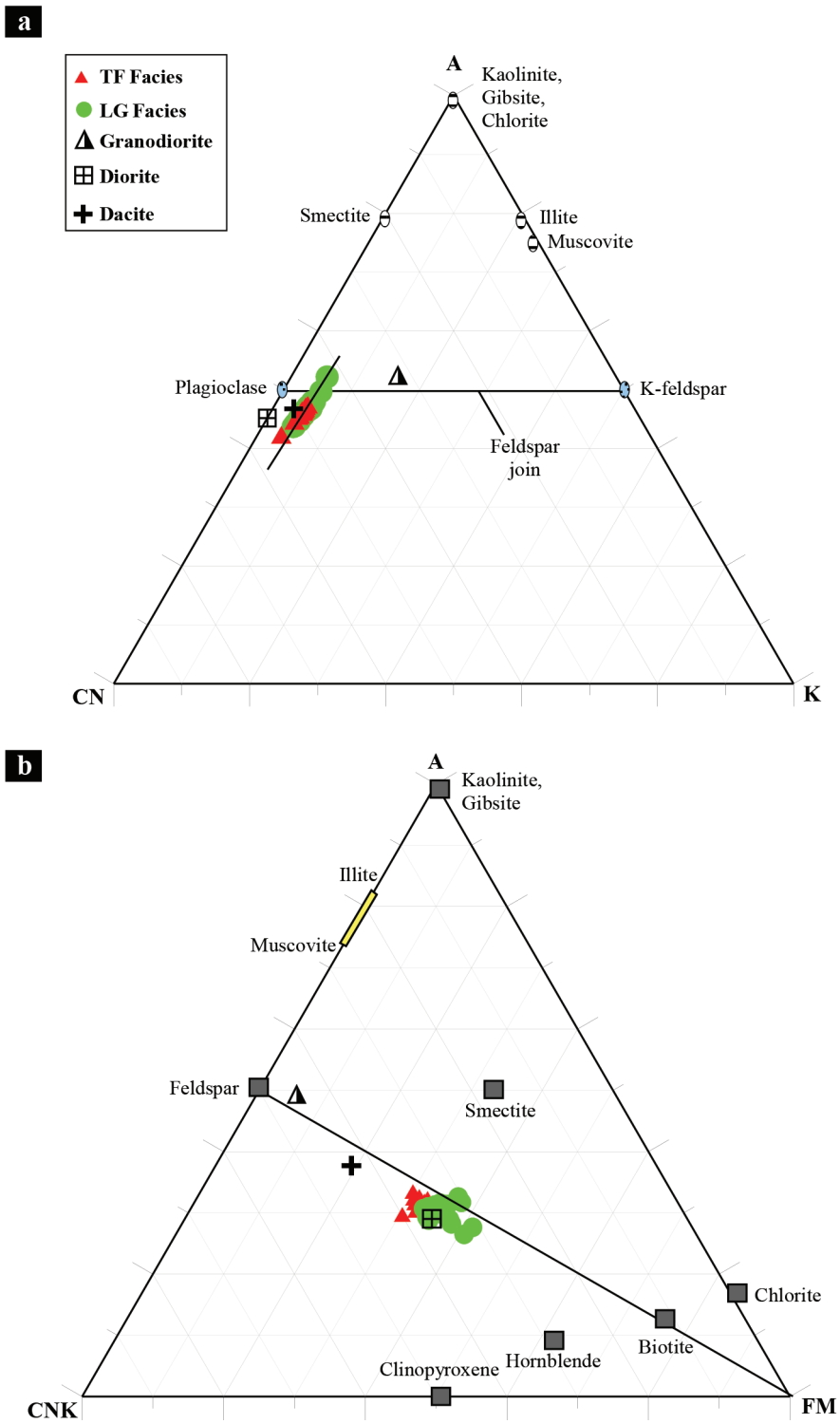

Figure 10. Paleoweathering ternary diagrams (after Nesbit and Young, 1984, 1989). a) The A-CN-K diagram with samples plotting below the feldspar join and weathering trend running parallel with the A-CN edge, indicating unweathered to poorly weathered sediments. b) A-CNK-FM diagram showing the weathering trend of the sediments. The sediments plot in an area of similar composition of unweathered dioritic source rock. For comparison, geochemical data from Hijaz Terrane (Brown et al., 1989) are used (A = Al_2O_3; C = CaO; N = Na_2O; K = K_2O; F = Fe_2O_3; M = MgO).

The K/Rb ratio has been employed to determine the degree of weathering. The K/Rb ratio varied between 296 and 460 (Table 2; Figure 5). This ratio is high compared to the ratio in UCC (230; Wronkiewicks and Condie, 1990). These high ratios indicate that the K-bearing minerals are poorly weathered.

The overall synthesis of geochemical and mineralogical data of the shallow subsurface sediments south of Al-Kharrar Lagoon suggests that the source rocks were affected by accelerated physical rather than chemical erosion. The bivariate plot of (Al_2O_3+K_2O+Na_2O) % vs. SiO_2% was used to interpret the climatic conditions under which the sediments were produced (Suttner and Dutta, 1986). The samples were plotted in the field of arid climate (Figure 11). This arid climate is consistent with low values of paleoweathering indices and the dominant arid climate that prevailed in Arabia and North Africa during the late Holocene. Following the Early Holocene, a humid period continued until 6 ka BP and an interval of aridity then prevailed until the present (Parker et al., 2006; Wellbrock et al., 2011; Engel et al., 2012; Rosenberg et al., 2013). Abu-Zied and Bantan (2015) attributed the barren interval at the base of the Al-Shuaiba core, along the Red Sea coast, to the dominance of arid climate and fall in sea level at about 1500 BC. This event corresponds to a regional period of maximum aridity (4.4 to 3.3 ka BP) that was recorded in deep-sea sediments from the central and northern Red Sea (Arz et al., 2006; Legge et al., 2006; Edelman-Furstenberg et al., 2009). In a recent study, Bantan et al. (2019), based on the vertical variation in benthic foraminiferal assemblages, suggested a generally warm and arid climate in the last 5500 years for the area of the Al-Kharrar Lagoon. This warm period is punctuated with a cooling event around AD 1500–1750 corresponding to the Little Ice Age (Bantan et al., 2019).

5.3. Hydraulic sorting

There are no obvious changes in the composition of source rock through time and there is also no evidence of changing weathering. This leaves hydraulic sorting the most likely reason for the slight variation in elemental concentrations in the two facies. Hydraulic sorting of sediments during transportation and deposition is an important parameter among other parameters that control the chemical and mineralogical composition of sediments (Ghandour et al., 2003; Weltje and von Eynatten, 2004; Garzanti et al., 2010; Lupker et al., 2011; Jian et al., 2013). Hydraulic sorting is controlled by grain size, shape, and density. The variation in the hydraulic sorting leads to mineralogical differentiation and chemical heterogeneity. An elemental ratio such as Al/Si can be used to illustrate the influence of hydraulic sorting as Si occurs commonly in the coarser fraction that is enriched in quartz and feldspars, whereas Al is a commonly formed mineral in phyllosilicates and clay minerals (Bouchez et al., 2011; Lupker et al., 2013; Pang et al., 2018). Therefore, high Al/Si ratios characterize fine-grained, clay-rich sediments, whereas low ratios indicate coarse-grained quartz-rich sediments. The Al/Si ratio for the sediments of facies LG ranges between 0.29 and 0.39 (average: 0.34) and from 0.28 to 0.3 (average: 0.29) for the sediments of facies TF (Table 2; Figure 5). The upcore decrease in the Al/Si ratio is consistent with the regressive pattern of the facies. When a pile of sediments derived from a similar source was transported into the lagoonal system, hydraulic sorting differentially concentrated quartz-rich sandy sediments in the nearshore shallow area and drifted clay-rich muddy sediments into deeper and calmer sites. A slight increase in the CIA and PIA values in the sediments of facies LG compared with those in facies TF can possibly be attributed to the relative abundance of phyllosilicates rather than the increase in the degree of weathering.

5.4. Redox conditions

The sediments of the LG facies are gray and relatively enriched in organic carbon, which may suggest deposition under oxygen-depleted conditions. Understanding the enrichment level and the distribution of the redox-sensitive trace elements (V, Cr, Cu, and Zn) is crucial to interpret the redox conditions under which the sediments under investigation were deposited. These elements are easily dissolved under oxic conditions and are less soluble under suboxic to anoxic environments (Tribovillard et al., 2006; März et al., 2008). They are therefore enriched under oxygen-depleted conditions. Values of V/Cr ratio of less than 2 refer to oxic bottom conditions, values of 2.0–4.25 indicate dysoxic conditions, and values higher than 4.25 characterize suboxic to anoxic conditions (Jones and Manning, 1994; Rimmer, 2004). The V/Cr ratios of lagoonal sediments are generally less than 2, varying from 1.43 to 1.71 (average: 1.58), whereas the average V/Cr ratio in the sediments of the TF facies is 1.6 (Table 2; Figure 5). Similarly, the Cu/Zn ratio has been utilized as a paleoredox indicator. Copper is reduced to Cu(I) under reducing conditions and may be incorporated in solid solution in pyrite or may even form its sulfide phases (CuS and CuS_2) (Huerta-Diaz and Morse, 1990). Values of Cu/Zn ratio of >1 indicate reducing conditions and low values refer to oxidizing conditions (Goldberg and Humayun, 2016; Tobia and Shangola, 2016). The Cu/Zn ratio was generally low (<1) in the core sediments; however, the Cu/Zn ratio in the sediments of the LG facies are slightly higher than their counterparts in the sediments of the TF facies (Table 2; Figure 5). The low V/Cr and Cu/Zn values suggest that lagoonal sediments were deposited under oxic bottom conditions. The slightly enriched V and Cr (by factors of 2 or 3) are therefore related to the presence of V- and Cr-bearing heavy minerals rather than the dysoxic or anoxic bottom water of the Al-Kharrar paleolagoon.

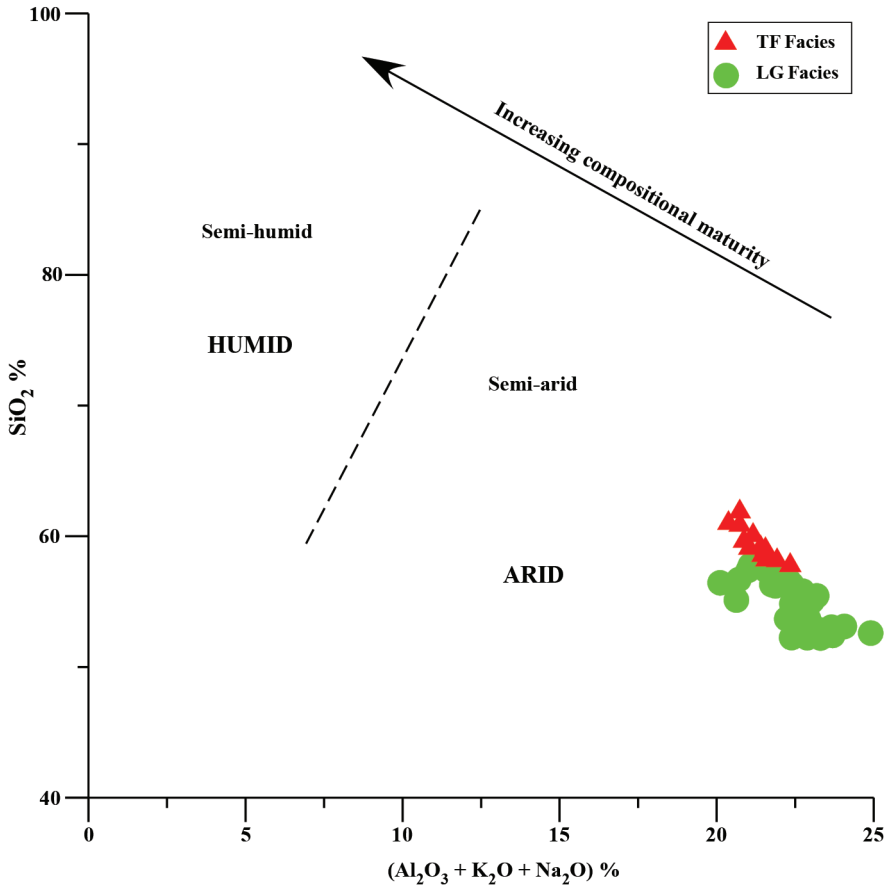

Figure 11. The $(Al_2O_3+K_2O+Na_2O)$ % vs. SiO_2% paleoclimate discrimination diagram (after Suttner and Dutta, 1986). The sediments of the two facies display similar paleoclimatic arid trends.

Under anoxic conditions, redox-sensitive elements are strongly enriched by factors of up to 100 or more (März et al., 2008).

6. Conclusions

The sedimentology of a short sediment core (2.05 m long) collected from the southern tidal flat of the Al-Kharrar Lagoon, Rabigh area, Saudi Arabia, showed two vertically stacked sedimentary facies: lagoonal (LG) gray silt-rich mud to argillaceous very fine sand at the base and intertidal flat (TF) brown mud and argillaceous very fine-grained sands at the top. Mineralogical and geochemical data of these sediments enabled distinguishing major controls on the abundance and distribution patterns of minerals and elements. The concluding remarks are summarized as follows:

1- The sediments of the two facies differ slightly in their mineralogical and chemical compositions. They are dominantly siliciclastic, consisting mainly of detrital minerals quartz, feldspars, and clay minerals occasionally mixed with traces of amphiboles, carbonates, and evaporite minerals.

2- Geochemically, the sediments are first-cycle and immature. The values of the Al_2O_3/TiO_2 ratio and the bivariate plots of Zr-TiO_2 and K_2O-Rb indicated that the sediments were derived from intermediate igneous rocks of the Birak group that is widely distributed in the intraoceanic island arc of the Hijaz Terrane, western Arabian Shield.

3- The average values of paleoweathering indices CIA, CIW, and PIA were generally less than 50, suggesting an unweathered to poorly weathered source rock. The poor weathering effect is compatible with the late Holocene arid climate.

4- The values of the redox-sensitive V/Cr (<2) and Cu/Zn (<1) ratios for the sediments of the lagoonal facies indicated deposition under oxic bottom conditions.

5- The mineralogical and chemical characteristics of the shallow subsurface late Holocene sediments south of Al-Kharrar Lagoon were mainly controlled by the source

rock composition and to a lesser extent hydraulic sorting, whereas the roles of climate and environmental conditions were minimal and negligible.

Acknowledgments
This project was funded by the Deanship of Scientific Research (DSR) at King Abdulaziz University, Jeddah, under Grant No. G-366-150-37. The authors thank the DSR for this technical and financial support. We would like to thank Prof. R. Alagarsamy (CSIR-National Institute of Oceanography, Goa, India) for reading and improving the language of the manuscript. We are very grateful to the editors and the reviewers for their constructive comments and editorial handling.

References

Abou-Ouf M (1996). Variation of benthic foraminiferal assemblages in different microenvironments along the shore zone north of Rabigh coast, eastern Red Sea, Saudi Arabia. Neues Jahrbuch für Geologie und Paläontologie P-A 3: 129-139.

Abu-Zied RH, Bantan RA (2015). Palaeoenvironment, palaeoclimate and sea-level changes in the Shuaiba Lagoon during the late Holocene (last 3.6 ka), eastern Red Sea coast, Saudi Arabia. Holocene 25: 1301-1312.

Al-Dubai TA, Abu-Zied RH, Basaham AS (2017). Diversity and distribution of benthic foraminifera in the Al-Kharrar Lagoon, eastern Red Sea coast, Saudi Arabia. Micropaleontology 63: 275-303.

Al-Washmi HA (1999). Sedimentological aspects and environmental conditions recognized from the bottom sediments of Al-Kharrar Lagoon, Eastern Red Sea Coastal Plain, Saudi Arabia. Journal of King Abdulaziz University - Marine Sciences 10: 71- 87.

Aref M, Attiia O, Wali A (1997). Facies and depositional environment of the Holocene evaporites in the Ras Shukeir area, Gulf of Suez, Egypt. Sedimentary Geology 110: 123-145.

Aref M, Taj R (2018). Recent evaporite deposition associated with microbial mats, Al-Kharrar supratidal–intertidal sabkha, Rabigh area, Red Sea coastal plain of Saudi Arabia. Facies 64: 28. doi: 10.1007/s10347-018-0539-y

Arz HW, Lamy F, Pätzold J (2006). A pronounced dry event recorded around 4.2 ka in brine sediments from the northern Red Sea. Quaternary Research 66: 432-441. doi: 10.1016/j.yqres.2006.05.006

Bailey GN, Flemming N, King GCP, Lambeck K, Momber G et al. (2007). Coastlines, submerged landscapes and human evolution: the Red Sea Basin and the Farasan Islands. Journal of Island and Coastal Archaeology 2: 127-160.

Bamousa AO (2013). Complex tectonic history of Al-Yutamah Dome Area within Hijaz Terrane, Arabian Shield, south of Al Madinah, Saudi Arabia. Open Geology Journal 7: 45-53.

Bantan RA, Abu-Zied RH, Al-Dubai TA (2019). Late Holocene environmental changes in a sediment core from Al-Kharrar Lagoon, Eastern Red Sea Coast, Saudi Arabia. Arabian Journal for Science and Engineering 44: 6557- 6570. doi: 10.1007/s13369-019-03958-9

Basaham AS (2008). Mineralogical and chemical composition of the mud fraction from the surface sediments of Sharm Al-Kharrar, a Red Sea coastal lagoon. Oceanologia 50: 557-575.

Basaham AS, El Sayed MA, Ghandour IM, Masuda H (2015). Geochemical background for the Saudi Red Sea coastal systems and its implication for future environmental monitoring and assessment. Environmental Earth Sciences 74: 4561-4570. doi: 10.1007/s12665-015-4477-5

Behairy AKA, Durgaprasada Rao NVN, El-Shater A (1991). A siliciclastic coastal Sabkha, Red Sea, Saudi Arabia. Journal of King Abdulaziz University - Marine Sciences 2: 65-77.

Bhatia MR (1983). Plate tectonics and geochemical composition of sandstones. Journal of Geology 91: 611-627.

Blatt H, Middleton GV, Murray RC (editors) (1980). Origin of Sedimentary Rocks. 2nd Edition. Upper Saddle River, NJ, USA: Prentice Hall.

Bouchez J, Gaillardet J, France-Lanord C, Maurice L, Dutra-Maia P (2011). Grain size control of river suspended sediment geochemistry: clues from Amazon River depth profiles. Geochemistry, Geophysics, Geosystems 12: 1-24 doi: 10.1029/2010GC003380

Brown GF, Schmidt DL, Huffman AC (1989). Geology of the Arabian Peninsula, Shield Area of Western Saudi Arabia. U.S. Geological Survey Professional Paper 560-A. Washington, DC, USA: USGS.

Calvert SE, Pedersen TF (1993). Geochemistry of recent oxic and anoxic marine sediments: implications for the geological record. Marine Geology 113: 67-88.

Chen Q, Liu Z, Kissel C (2017). Clay mineralogical and geochemical proxies of the East Asian summer monsoon evolution in the South China Sea during Late Quaternary. Scientific Reports 7: 1-9.

Cox R, Lowe DR, Cullers RL (1995). The influence of sediment recycling and basement composition on evolution of mud rock chemistry in the South-western United States. Geochimica et Cosmochimica Acta 59: 2919-2940.

Cruces A, Freitas MC, Andrade C, Munhá J, Tassinari C et al. (2006). The importance of geochemistry in multidisciplinary studies of lagoonal environments at different time scales: the case of Santo André lagoon (SW Portugal). Journal of Coastal Research Special Issue 39: 1716-1722.

Cui Z, Schulz-Bull DE, Hou Y, Xia Z, Waniek JJ (2016). Geochemical Characteristics and Provenance of Holocene Sediments (Core STAT22) in the Beibu Gulf, South China Sea. Journal of Coastal Research 32: 1105-1115. doi: 10.2112/JCOASTRES-D-14-00238.1

Edelman-Furstenberg Y, Almogi-Labin A, Hemleben C (2009). Paleoceanographic evolution of central Red Sea during the late Holocene. Holocene 19: 117-127.

El-Abd Y, Awad MB (1991). Evaporitic sediment distributions in Al-Kharrar sabkha, west Red Sea of Saudi Arabia, as revealed from the electrical soundings. Marine Geology 97: 137-143.

Engel M, Brückner H, Pint A, Wellbrock K, Ginau A et al. (2012). The Early Holocene humid period in NW Saudi Arabia; sediments, microfossils and palaeo-hydrological modelling. Quaternary International 266: 131-141.

Fedo CM, Nesbitt HW, Young GM (1995). Unraveling the effects of potassium metasomatism in sedimentary rocks and paleosols, with implications for paleoweathering conditions and provenance. Geology 23: 921-924.

Floyd P, Leveridge B (1987). Tectonic environment of the Devonian Gramscatho basin, south Cornwall: framework mode and geochemical evidence from turbiditic sandstones. Geological Society of London 144: 531-540.

Garzanti E, Ando S, France-Lanord C, Vezzoli G, Censi P et al. (2010). Mineralogical and chemical variability of fluvial sediments: 1. Bedload sand (Ganga–Brahmaputra, Bangladesh). Earth and Planetary Science Letters 299: 368-381.

Ge Q, Xue GZ, Ye L, Xu D, Zhao J et al. (2019). The spatial distribution of major and trace elements of surface sediments in the northeastern Beibu Gulf of the South China Sea. Acta Oceanologica Sinica 38: 93-102. doi: 10.1007/s13131-019-1402-x

Ghandour IM, Al-Washmi HA, Haredy RA, Zubairi A (2016). Facies evolution and depositional model of an arid microtidal coast: example from the coastal plain at the mouth of Wadi Al-Hamd, Red Sea, Saudi Arabia. Turkish Journal of Earth Sciences 25: 256-273.

Ghandour IM, Basaham A, Haredy R, Manaa A, Al-Rabaki K et al. (2019). Geochemistry of the Gulf of Aden Beach Sands, Al-Mukalla, Yemen: provenance and tectonic setting implications. Acta Geodynamica et Geomaterialia 16: 55-69.

Ghandour IM, Haredy RA (2019). Facies analysis and sequence stratigraphy of Al-Kharrar Lagoon coastal sediments, Rabigh area, Saudi Arabia: impact of sea level and climate changes on coastal evolution. Arabian Journal for Science and Engineering 44: 505-520. doi: 10.1007/s13369-018-3662-8

Ghandour IM, Masuda H, Maejima W (2003). Mineralogical and chemical characteristics of Bajocian – Bathonian shales, G. Al-Maghara, North Sinai, Egypt: Climatic and environmental significance. Geochemical Journal 37: 87-108.

Goldberg K, Humayun M (2016). Geochemical paleoredox indicators in organic-rich shales of the Irati Formation, Permian of the Paraná Basin, southern Brazil. Brazilian Journal of Geology 46: 377-393.

Guo Y, Yang S, Sua N, Li C, Yin P et al. (2018). Revisiting the effects of hydrodynamic sorting and sedimentary recycling on chemical weathering indices. Geochimica et Cosmochimica Acta 227: 48-63.

Hardy R, Tucker M (1988). X-ray powder diffraction of sediments. In: Tucker M (editor). Techniques in Sedimentology. Oxford, UK: Blackwell Scientific Publications, pp. 191-228.

Hargrove US, Stern RJ, Griffin WR, Johnson PR, Abdelsalam MG (2006). From Island Arc to Craton: Timescales of Crustal Formation along the Neoproterozoic Bi'r Umq Suture Zone, Kingdom of Saudi Arabia. Technical Report SGS-TR-2006-6: 69. Jeddah, Saudi Arabia: Saudi Geological Survey.

Hariri MSB, Abu-Zeid RH (2018). Factors influencing heavy metal concentrations in the bottom sediments of the Al-Kharrar Lagoon and Salman Bay, eastern Red Sea coast, Saudi Arabia. Arabian Journal of Geosciences 11: 495. doi: 10.1007/s12517-018-3838-2

Harnois L (1988). The CIW index: A new chemical index of weathering. Sedimentary Geology 55: 319-322.

Hayashi KI, Fujisawa H, Holland HD, Ohomoto H (1997). Geochemistry of ~1.9 Ga sedimentary rocks from northern Labrador, Canada. Geochemica et Cosmochemica Acta 61: 4115-4137.

Hein CJ, Fitzgerald DM, Milne GA, Bard K, Fattovich R (2011). Evolution of a Pharaonic harbor on the Red Sea: implications for coastal response to changes in sea-level and climate. Geology 39: 687-690.

Heiri O, Lotter AF, Lemcke G (2001). Loss on ignition as a method for estimating organic and carbonate content in sediments: reproducibility and comparability of results. Journal of Paleolimnology 25: 101-110.

Huerta-Diaz MA, Morse JW (1990). A quantitative method for determination of trace metal concentrations in sedimentary pyrite. Marine Chemistry 29: 119-144.

Jian X, Guan P, Zhang W, Feng F (2013). Geochemistry of Mesozoic and Cenozoic sediments in the northern Qaidam basin, northeastern Tibetan Plateau: implications for provenance and weathering. Chemical Geology 360-361: 74-88.

Johnson PR (2006). Explanatory Notes to the Map of Proterozoic Geology of Western Saudi Arabia: Saudi Geological Survey Technical Report, SGS-TR-2006-4: 62. Jeddah, Saudi Arabia: Saudi Geological Survey.

Johnson PR, Abdelsalam MG, Stern RJ (2003). The Bi'r Umq suture zone in the Arabian-Nubian shield: a key to understanding crustal growth in the East African Orogen. Gondwana Research 6: 523-530.

Jones B, Manning DAC (1994). Comparison of geochemical indices used for the interpretation of palaeoredox conditions in ancient mudstones. Chemical Geology 111: 111-129.

Legge HL, Mutterlose J, Arz HW (2006). Climatic changes in the northern Red Sea during the last 22,000 years as recorded by calcareous nannofossil. Paleoceanography 21: 1-16.

Li YH, Schoonmaker JE (2003). Chemical composition and mineralogy of marine sediments. In: Holland HD, Turekian KK (editors). Treatise on Geochemistry. Amsterdam, the Netherlands: Elsevier, pp. 3469-3503.

Lindsey DA (1999). An Evaluation of Alternative Chemical Classifications of Sandstones. U.S. Geological Survey Open File Report 99-346. Washington, DC, USA: USGS.

Liu X, Rendle-Bühring R, Henrich R (2017). Geochemical composition of Tanzanian shelf sediments indicates Holocene climatic and sea-level changes. Quaternary Research 87: 442-454.

Lü X, Versteegh GJM, Song J, Li X, Yuan H et al. (2016). Geochemistry of Middle Holocene sediments from south Yellow Sea: implications to provenance and climate change. Journal of Earth Science 27: 751-762.

Lupker, M, France-Lanord, C, Galy, V, Lavé, J, Kudrass, H (2013). Increasing chemical weathering in the Himalayan system since the Last Glacial Maximum. Earth and Planetary Science Letters 365: 243-252.

Lupker M, France-Lanord C, Lave J, Bouchez J, Galy V et al. (2011). A Rouse-based method to integrate the chemical composition of river sediments: application to the Ganga basin. Journal of Geophysical Research 116: 1-24.

Marco-Barba J, Holmes JA, Mesquita-Joanes F, Miracle MR (2013). The influence of climate and sea-level change on the Holocene evolution of a Mediterranean coastal lagoon: evidence from ostracod palaeoecology and geochemistry. Geobios 46: 409-421.

Martín-Puertas C, Jiménez-Espejo F, Martínez-Ruiz F, Nieto-Moreno V, Rodrigo M et al. (2010). Late Holocene climate variability in the southwestern Mediterranean region: an integrated marine and terrestrial geochemical approach. Climate of the Past 6: 807-816.

März C, Poulton SW, Beckmann B, Küster K, Wagner T et al. (2008). Redox sensitivity of P cycling during marine black shale formation: dynamics of sulfidic and anoxic, non-sulfidic bottom waters. Geochimica et Cosmochimica Acta 72: 3703-3717. doi: 10.1016/j.gca.2008.04.025

McLennan SM (1993). Weathering and global denudation. Journal of Geology 101: 295-303.

Moore DM, Reynolds RC (1989). X-ray Diffraction and the Identification and Analysis of Clay Minerals. Oxford, UK: Oxford University Press.

Nesbitt HW, Fedo CM, Young GM (1997). Quartz and feldspar stability, steady and non-steady-state weathering, and petrogenesis of siliciclastic sands and muds. Geology 105: 173-191.

Nesbitt HW, Young GM (1982). Early Proterozoic climates and plate motions inferred from major element chemistry of lutites. Nature 299: 715-717.

Nesbitt HW, Young GM (1984). Prediction of some weathering trends of plutonic and volcanic rocks based on thermodynamic and kinetic considerations. Geohemica et Cosmochemica Acta 48: 1523-1534.

Nesbitt HW, Young GM (1989). Formation and diagenesis of weathering profiles. Geology 97: 129-147.

Nesbitt HW, Young GM (1996). Petrogenesis of sediments in the absence of chemical weathering: effects of abrasion and sorting on bulk composition and mineralogy. Sedimentology 43: 341-358.

Ohta T, Arai H (2007). Statistical empirical index of chemical weathering in igneous rocks: a new tool for evaluating the degree of weathering. Chemical Geology 240: 280-297.

Pang H, Pan B, Garzanti E, Gao H, Zhao X et al. (2018). Mineralogy and geochemistry of modern Yellow River sediments: Implications for weathering and provenance. Chemical Geology 488: 76-86.

Parker AG, Goudie AS, Stokes S, White K, Hodson MJ et al. (2006). A record of Holocene climate change from lake geochemical analyses in southeastern Arabia. Quaternary Research 66: 465-476.

Pettijohn FJ, Potter PE, Siever R (1972). Sand and Sandstones. New York, NY, USA: Springer-Verlag.

Ramsay CR (1986). Explanatory Notes to the Geologic Map of the Rabigh Quadrangle, Sheet 22D. Jeddah, Saudi Arabia: Saudi Geological Survey.

Rasul NMA (2015). Lagoon sediments of the Eastern Red Sea: distribution processes, pathways and patterns. In: Rasul NMA, Stewart ICF (editors). The Red Sea. Earth System Sciences. Berlin, Germany: Springer, pp. 281-316.

Reotita J, Siringan F, Zhang J, Azanza R (2014). Paleoenvironment changes in Juag Lagoon, Philippines based on sedimentology, bulk geochemistry and stable isotopes and their implication to nitrification. Quaternary International 333: 110-121.

Rimmer SM (2004). Geochemical paleoredox indicators in Devonian–Mississippian black shales, Central Appalachian Basin (USA). Chemical Geology 206: 373-391.

Rosenberg TM, Preusser F, Risberg J, Plikk A, Kadi KA et al. (2013). Middle and Late Pleistocene humid periods recorded in palaeolake deposits of the Nafud desert, Saudi Arabia. Quaternary Science Review 70: 109-123.

Roser BP, Korsch RJ (1986). Determination of tectonic setting of sandstone–mudstone unites using SiO_2 content and K_2O/Na_2O ratio. Geology 94: 635-650.

Roser BP, Korsch RJ (1988). Provenance signatures of sandstone–mudstone suites determined using discriminant function analysis of major-element data. Chemical Geology 67: 119-139.

Sawant SS, Kumar KV, Balaram V, Subba-Rao DV, Rao KS et al. (2017) Geochemistry and genesis of craton-derived sediments from active continental margins: insights from the Mizoram Foreland Basin, NE India. Chemical Geology 470: 13-32.

Siegel FR, Gupta N, Shergill B, Stanley DJ, Gerber C (1995). Geochemistry of Holocene sediments from the Nile Delta. Journal of Coastal Research 11: 415-431.

Suttner LJ, Dutta PK (1986). Alluvial sandstone composition and palaeoclimate, I. Framework mineralogy. Journal of Sedimentary Petrology 56: 329-345.

Tawfik HA, Ghandour IM, Maejima W, Armstrong-Altrin JS, Abdel-Hameed AT (2017). Petrography and geochemistry of the siliciclastic Araba Formation (Cambrian), east Sinai, Egypt: implications for provenance, tectonic setting and source weathering. Geological Magazine 154: 1-23.

Taylor SR, McLennan SM (1985). The Continental Crust: Its Composition and Evolution. Oxford, UK: Blackwell Scientific Publications.

Tobia FH, Shangola SS (2016). Mineralogy, geochemistry, and depositional environment of the Beduh Shale (Lower Triassic), Northern Thrust Zone, Iraq. Turkish Journal of Earth Sciences 25: 367-391.

Tribovillard N, Algeo TJ, Lyons T, Riboulleau, A (2006). Trace metals as paleoredox and paleoproductivity proxies: an update. Chemical Geology 232:12-32.

Tribovillard N, Koched H, Baudin F, Adatte T, Delattre M et al. (2019). Storm-induced concentration of sulfurized, marine-origin, organic matter as a possible mechanism in the formation of petroleum source-rock. Marine and Petroleum Geology 109: 808-818.

Wellbrock K, Voss P, Grottker M (2011). Reconstruction of mid-Holocene climate conditions for north-western Arabian oasis Tayma. International Journal Water Resources and Arid Environments 1: 200-209.

Weltje GJ, Von-Eynatten H (2004). Quantitative provenance analysis of sediments: review and outlook. Sedimentary Geology 171: 1-11.

Wronkiewicz DJ, Condie KC (1987). Geochemistry of Archean shales from the Witwatersrand Supergroup, South Africa: source-area weathering and provenance. Geochemica et Cosmochemica Acta 51: 2401-2416.

Yan Z, Wang Z, Yan Q, Wang T, Guo X (2012). Geochemical constraints on the provenance and depositional setting of the Devonian Liuling Group, East Qinling Mountains, Central China: implications for the tectonic evolution of the Qinling Orogenic Belt. Journal of Sedimentary Research 82: 9-24.

Zaigham NA, Aburizaiza OS, Mahar GA, Nayyer ZA, Siddique A (2015). Watershed analysis of Rabigh Drainage Basin, Saudi Arabia. International Journal of Water Resources and Arid Environments 4: 138-145.